Department of Precision and Microsystems Engineering

Compliant Activatable Neutrally Stable Joint

Hanzalah Ahmad

Report no : 2022.001
Coach : Dr. ir. G. Radaelli
Professor : Prof. dr. ir. J.L. Herder
Specialisation : Mechatronic System Design
Type of report : Thesis
Date : 25-01-2022

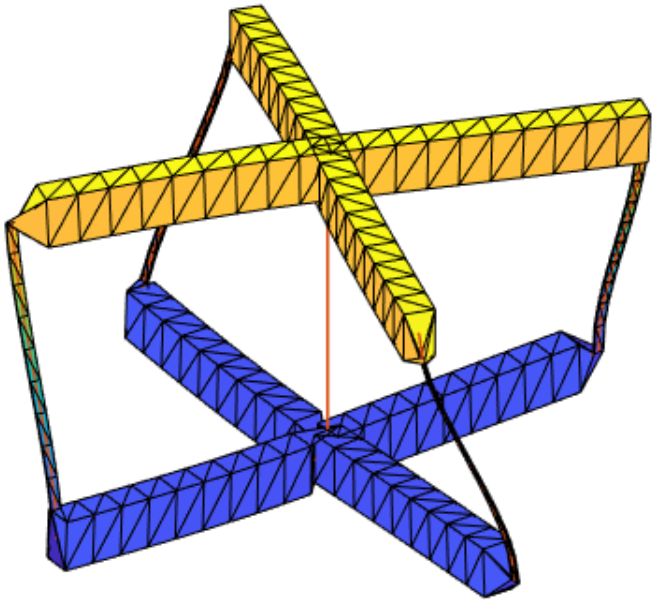

Compliant Activatable Neutrally Stable Joint

by

Hanzalah Ahmad

to obtain the degree of Master of Science
at the Delft University of Technology,
to be defended publicly on Tuesday January 25, 2022 at 12:30 PM.

Student number:	4567471	
Project duration:	September, 2020 – January, 2022	
Thesis committee:	Dr. ir. G. Radaelli,	TU Delft, supervisor
	Prof. dr. ir. J. L. Herder,	TU Delft, chair
	Ir. W. van de Sande,	TU Delft

TU Delft

Preface

As far as I can remember, I have always been interested in machines and technology. Whenever I saw something new, the first thing I would ask is; how does it work? This eagerness to find out how things work led me to engineering. Many years later, I am now about to graduate in Mechanical Engineering. In the past year, I have been working on this small mechanism, which may be a tiny thing in the grand world of engineering, but it has shown me why I like machines and technology. The logic and the simplicity of certain concepts which are the basis of complex machines - both on nanoscopic scale as well as macroscopic scale - is what makes this field so fascinating and interesting.

This thesis report is the result of five and half years studying, in which everything I have learned about engineering comes together. And I am glad I chose this path, because I have not only acquired skills which will be useful in my professional career, but I have also grown as a person. And although this thesis marks the end of my wonderful academic career, I am certain that it is also the beginning of a professional career in which I will still learn a lot.

Hanzalah Ahmad
Amstelveen, January 2022

Contents

I

Thesis

1

Introduction

Compliant mechanisms are mechanisms that use the flexibility of their members to elastically deform contrary to traditional mechanisms that use stiff and rigid parts with hinges [6]. A major advantage of compliant mechanisms is that the total number of parts is significantly less than traditional mechanisms. Compliant mechanisms have less wear and backlash and are more precise. Moreover, they are easier to manufacture and can be used for applications on both the micro scale as well as the macro scale [1],[6].

There are many different mechanisms and devices that can be identified as compliant mechanisms. One class of compliant mechanisms are neutrally stable compliant mechanisms. Neutrally stable compliant mechanisms can undergo large elastic deformation and maintain the deformed configuration without the need for external work [10]. These neutrally stable compliant mechanisms require some sort of pre-stress to reach the neutrally stable state. The disadvantage to this is, that this pre-stress is mostly applied when the neutrally stable mechanisms are being made [3], [5] & [8]. Therefore, these mechanisms are always in a neutrally stable state. Furthermore, when a compliant mechanism is exposed to too much stress over a longer period of time, it can lead to creep [4].

Therefore, it is desired to find a system in which this stress can be turned on and off when required, i.e., a compliant mechanism that can switch between a stiff state and a neutrally stable state. Such a mechanism can for instance be used to transport a satellite with solar panels to its orbit around the world. During transportation, the solar panels are folded, for which the joints of the solar panels need to be in a stiff state. In orbit, the solar panels are unfolded, for which the joints should be neutrally stable.

Joosten et al. [7] have made a compliant Hygromorphic Rotational Actuator (HRA) which may be a solution to the previously stated problem. The HRA is a rotational wooden actuator that shows neutrally stable behavior when it is made wet (activated). This neutrally stable behavior was however not the main focus of the paper. Moreover, since the activation of the HRA is realized by absorption of moisture by wood, this actuator has a limited lifetime of only two or three cycles, since moisture absorption is not completely reversible. This also means that after the HRA has rotated once, it does not completely move back to its original position. However, the activatable behavior aspect of the actuator does provide opportunities for the pre-stress to be turned and off in neutrally stable mechanisms.

This thesis report focuses on the neutrally stable behavior of compliant mechanisms. In particular, the neutrally stable behavior generated by rotational motion based on the HRA [7]. The goal of this thesis is to make an activatable neutrally stable compliant mechanism, i.e. a compliant mechanism that can switch between a stiff state and a neutrally stable state whenever required. This will also remove the issue of excessive stress exposure. This is realized by using a Flexinol SMA wire. When heated, the Flexinol wire will contract and if it is cooled, it will elongate back to its original length. This activatable behavior of the Flexinol wire is used to turn on and off the pre-stress whenever it is required.

1.1. Thesis outline

The main work of this thesis is the paper presented in chapter 2. In this paper, it is explained how a new Compliant Activatable Neutrally Stable Joint (CANS-J) is made. This paper is followed by appendices in which more in-depth information is given about: Design, prototyping and fabrication (A), Theoretical Rotation (B), Simulation (C) and the Test Setup (D).

In appendix A, it is explained how the CANS-J was designed, how initial prototypes of the design were made and how the eventual design was fabricated. Appendix B explains how the model for the theoretical possible rotation is derived based on the model of the HRA. In appendix C, it is explained how the CANS-J is simulated in Matlab. Appendix D gives information about how experiments on the CANS-J are done to verify the results from the simulation.

2

A Compliant Activatable Neutrally Stable Joint

Design and fabrication of a compliant joint with activatable pre-stress to switch between a stiff and a neutrally stable state.

Hanzalah Ahmad, Giuseppe Radaelli & Just Herder

***Abstract*—Neutrally stable compliant mechanisms are mechanisms that use the flexibility of their members to deform and maintain the deformed configuration without requiring external work. However, neutrally stable compliant mechanisms require some sort of pre-stress to become neutrally stable and thus cannot easily switch between the stiff state and the neutrally state. In this paper, a new Compliant Activatable Neutrally Stable Joint (CANS-J) is designed, simulated, fabricated and tested that can switch between a stiff state and a neutrally stable state using a Flexinol SMA wire. Simulations are done to determine which geometries show neutral stability behavior in the activated state. These geometries are then fabricated and tested in a torsion test bench and the torque during rotation is measured in both the non-activated and the activated state. In experiments, a clear neutral stability range is visible in the activated state which goes from 22 degrees to 50 degrees, which correspond to the simulations. The CANS-J provides opportunities for active materials to be used in neutrally stable compliant mechanisms.**

***Index Terms*—Active materials, compliant mechanisms, neutral stability, pre-stress, SMA wire.**

I. Introduction

Compliant mechanisms are mechanisms that use the flexibility of their members to elastically deform and generate motion, rather than using separate stiff and rigid parts with hinges. The main advantages of compliant mechanisms are: less parts, wear and backlash, more precision, no need for lubrication, easy to manufacture and the ability to manufacture MEMS devices [1]. The challenge of compliant mechanisms is that in order to elastically deform a member, external work is required. However, the ability to elastically deform can also be used to create a neutrally stable mechanism. A neutrally stable device can deform and stay in the deformed state, without the application of any external work [2].

Combining these two principles will lead to neutrally stable compliant mechanisms. There is already extensive research being done on neutrally stable compliant mechanisms. Neutrally stable compliant mechanisms require some sort of pre-stress to achieve the neutrally stable state. In most cases, this pre-stress is already applied when a neutrally stable compliant mechanism is made, meaning that the mechanism is always in a neutrally stable state [3], [4], [5], [6], [7] & [8]. In these examples, compliant mechanisms are made neutrally stable by buckling some of their members. The pre-stress is applied during fabrication to buckle the beams. As a consequence, the joints are always neutrally stable. Another disadvantage of applying pre-stress this way, is that over a period of time, the mechanisms will suffer from creep [9]. Consequently, after a while the neutral stability effect goes away. Therefore, it is desired to develop a neutrally stable compliant mechanism which can switch between the stiff state and the neutrally stable state by turning on and off the pre-stress.

A solution to this problem may be the compliant neutrally stable rotational actuator found in [10]. Joosten et al. [10] have made a Hygromorphic Rotational Actuator (HRA) of wood veneer that rotates when it is made wet, and when it is dry again, it goes back to its original state, see figure 1. Surprisingly, the actuator shows neutrally stable behavior in the wet state, meaning it can rotate and stay in the rotated state without the application of any external work. There are however a few disadvantages of the HRA: it has a limited lifetime of just two to three cycles and it does not completely move back to its original position when it is dry again, since moisture absorption is not a completely reversible process. However, the activatable behavior of the actuator does provide opportunities to tackle the problem of excessive stress exposure, i.e., active materials could be used to turn on and off the pre-stress required for the compliant neutrally stable mechanisms.

In this paper, a new Compliant Activatable Neutrally Stable Joint (CANS-J) based on the HRA is designed and fabricated. The main advantage of this joint is that the pres-stress can be turned on and off, so that the joint can switch between a stiff state and a neutrally stable state. Therefore, it is not continuously exposed to unnecessary stress. The activation of the pre-stress is realized using active materials. When the pre-stress is activated, the joint will show zero-stiffness when it is rotated. The design of CANS-J can be easily scaled to attain many ranges of motion.

In section II, it is explained how this new joint is designed, simulated, fabricated and tested. In the Results section, the results retrieved from the simulation and experiments are presented. This is followed by a Discussion section in which the results are discussed and the paper ends with Conclusions.

II. Methods

A. Design

In the HRA, when the wooden sheet is made wet, it wants to elongate in the vertical direction. However, this elongation is restricted along the centerline, h, and the upper and bottom edges of the wooden sheet, see figure 1. This elongation combined with the constraints causes the actuator to rotate.

The working principle of the CANS-J is somewhat similar to the working principle of HRA. In the CANS-J, the rotation is caused by contraction along the centerline, c, of the joint and restriction of movement on the vertical outer edges, see figure 2. The CANS-J is not made of a sheet, but flexures.

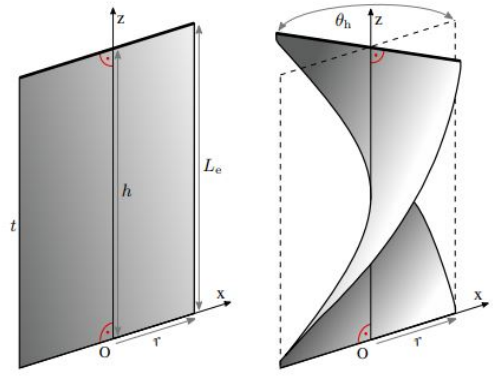

Fig. 1. Schematic view of the HRA in the dry (left) and wet (right) state, from [10].

Contraction in the center will apply a stress on the joint causing the flexures to buckle, resulting in the possibility to rotate. If the joint is now rotated, it will stay in the desired rotated state.

Since the main objective of the CANS-J is to turn on and off the pre-stress when required, a reversible active material is used. Active materials (or smart materials) are a type of material that can respond to external stimuli and change their physical properties as a response [11]. Reversible active materials can recover to their initial state, when the stimulus is removed.

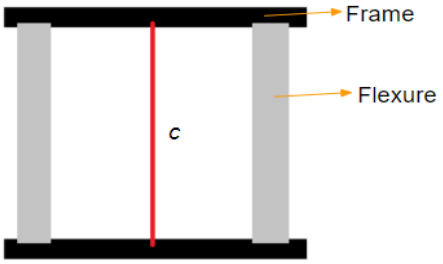

Fig. 2. Design of the CANS-J.

The active material used to turn on and off the pre-stress was chosen to be a Shape Memory Alloy (SMA) wire. SMA wires can change their shape when they are subjected to a heat stimulus [12]. Since the stress provided in the CANS-J is by way of contraction, Flexinol SMA wire was chosen, as it is already programmed to shrink along its length when it is heated and returns back to its original length when it is cooled.

The freedom to rotate when buckled combined with the stress provided by the contracted Flexinol wire, makes the joint neutrally stable. When the Flexinol wire is cooled, it elongates back to its original length, taking away the stress. This means that the flexures are unbuckled, making the joint stiff again and difficult to rotate. Thus, the CANS-J can switch between a stiff state and a neutrally stable state by simple heating and cooling of the Flexinol wire in the center. In others words, the stress can be turned on and off when required, taking away the problem of excessive stress exposure.

When the Flexinol wire is contracted, the flexures may buckle in the same direction. This will cause the joint to collapse. To prevent this from happening when the Flexinol wire is contracted, two of the aforementioned joints, see figure 2, are combined in a cross-like design with a 90 degrees of angle between them. This results in a design, which can be seen in figure 3.

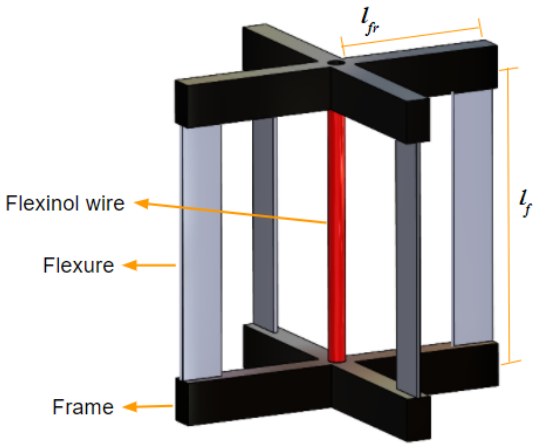

Fig. 3. 3D design of the the joint.

There are four key design parameters that define the geometry of the joint and have an influence on the performance of the joint. The width of the joint is defined by the length of the legs of the frame, l_{fr}, and the height of the joint is defined by the length of the flexures, l_f, see figure 3. Moreover, the width, w_f, and the thickness, t_f, of the flexures also have an influence on the performance of the joint.

B. Theoretical Rotation

Just like the HRA, in the deformed state the CANS-J will take a shape which resembles a helicoid. The authors of the HRA derived a model to determine the theoretical possible rotation of the HRA in the deformed state [10]. This model can also be used to determine the theoretical possible rotation of the CANS-J. However, since the helicoid shape is achieved by a contrary motion in the CANS-J, a different assumption is made.

In figure 4, it can be seen that a rolled-out helicoid takes the shape of a triangle. Each side of this triangle corresponds to the geometrical properties of the joint. h is the height of the joint, L is the length of the outer edges and C is the circumference of the helix. Using the Pythagorean theorem, the height, h, can be defined as follows:

$$h = \sqrt{L^2 - C^2} = \sqrt{L^2 - (2\pi)^2 \cdot r^2} \tag{1}$$

In CANS-J, the height, h, of the joint is driven by the length, L, of the outer edges and the contraction strain, S_h. This can

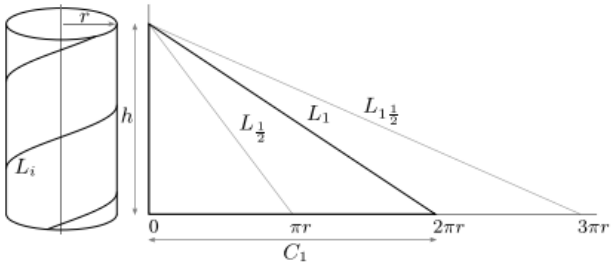

Fig. 4. A rolled-out helicoid, from [10].

Parameter	Value (in mm)
l_f	30 40 50 60 70 80
l_{fr}	10 15 20 25 25 30
w_f	1 2 3 4 5
t_f	0.1 0.2 0.3

TABLE I
VALUES THAT ARE SEARCHED FOR ALL THE 5 DESIGN PARAMETERS. ALL DIMENSIONS ARE IN mm.

be written as follows:

$$h = L \cdot (1 - S_h) \tag{2}$$

Substituting equation 2 in equation 1 and solving for 2π gives:

$$2\pi = \sqrt{\frac{L^2 - (L \cdot (1 - S_h))^2}{r^2}} \tag{3}$$

Replacing the parameters to match that of the CANS-J, the rotation angle in degrees can be calculated as follows:

$$\theta = \frac{180}{\pi} \sqrt{(2S_h - S_h^2)\frac{(l_f)^2}{(l_{fr})^2}} \tag{4}$$

From the equation, it can be seen that the height and the width of joint are the only two geometrical parameters that influence the rotation.

C. Simulation

A FEM analysis is done on the design using Matlab to determine which set of parameters gives the best result. This FEM analysis is done using a linear beam model based on the work of Battini [13]. The design is modeled by defining nodes along the frame and flexures of the geometry, where these nodes are connected with each other with elements, see figure 5. Every element in the simulation is modeled as a beam element of the Linear Beam Theory [14]. A linear material model is used in which it is assumed that the material is isotropic and uniform.

The number of nodes and thus elements can be increased to improve the accuracy of the result. In this simulation, each side of the joint is modelled using 10 elements. A convergence analysis was done to determine this number of elements. A slight geometrical offset is added to the top frame to make sure that the simulation is run. This is needed to overcome buckling. Thus, the center of the top frame is not perfectly above the centre of the bottom frame. A grid search is done to determine which values of the four design parameters give the desired behavior of neutral stability. Table I shows all the values of the four design parameter that were explored in the simulation. This gave a total of 540 different combinations of geometries.

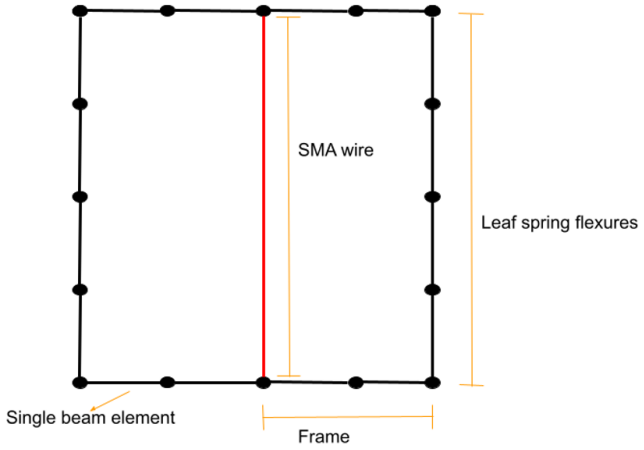

Fig. 5. Element view of the design.

There are 2 different simulations done: one of the activated state and one of the non-activated state. The simulation for the activated state is done as follows: the first step would be contracting the Flexinol with a strain of 4% and applying a rotation of angle, θ, as calculated using equation 4. However, for some dimensions this theoretical angle showed rotation which is too small to be of interest for this research. Therefore, a scaling factor of 1.5 is used in all the simulations. Thus, a scaled rotation, $\theta' = 1.5 \cdot \theta$, is applied on the center of the top frame, whilst the Flexinol wire is being contracted, see figure 6. Subsequently, a rotation of $-2\theta'$ is applied on the same location at the center of the top frame. Constraints on the center of the bottom frame are applied, which simulate a fixed state, preventing the the bottom frame of the joint from displacing when the SMA wire is contracted or when the rotations are applied, see figure 6. There is also a constraint applied on the center of the top frame to make sure that the top frame can only rotate and move up and down.

The simulation of the non-activated state has 2 differences from the simulation of the activated state. First, at the beginning of the simulation, the Flexinol wire is not contracted. Second, an extra movement constraint, a fixed support, is added to the top frame similar to the bottom frame. Thus, the top frame is prevented from moving up and down. This is done to minimize the differences with the experiments, as in

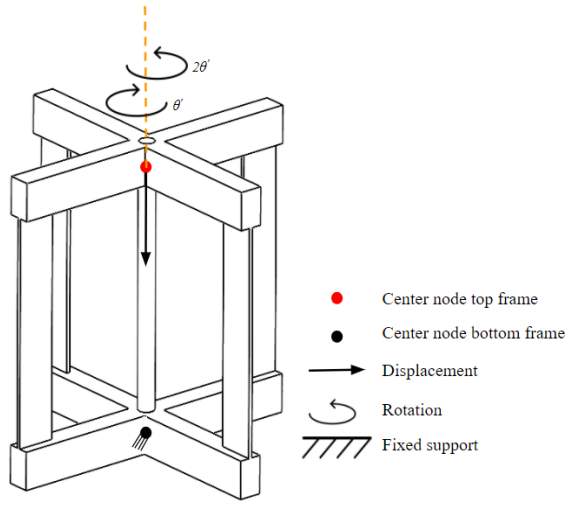

Fig. 6. Schematic view of the joint with all the boundary conditions used in the simulation.

the experiments the top frame is also restricted from moving up and down.

In the simulation, the reaction moment is measured during the second rotation at the centre of the bottom frame. From this reaction moment, torque-rotation graphs are made for all the different combinations of the geometries. From these graphs, five geometries were selected that showed neutrally stable behavior and fabricated to validate the simulation. The torque-angle graphs from the simulation of these five geometries are presented in section III. The dimensions corresponding to these results are shown in TABLE II.

Sample	l_f	l_{fr}	w_f	t_f
1	30	30	1	0.1
2	40	30	1	0.1
3	60	30	1	0.1
4	70	30	1	0.2
5	80	30	1	0.2

TABLE II
DIMENSIONS OF THE 5 RESULTING GEOMETRIES FROM THE SIMULATION. ALL DIMENSIONS ARE IN mm.

D. Prototype Fabrication

The five geometries that showed neutrally stable behavior found from the simulation were fabricated to validate the simulations.

For the flexures, steel leaf springs were chosen due to their flexure-like behavior and ease of manufacturing. An Optec microlaser cutter with a 15 Watt Talon UV nanosecond pulsed laser was used to lasercut the leaf springs corresponding to the dimensions retrieved from the simulations. The dimensions of the leaf springs are three of the four design parameters.

Since the objective is to turn on and off the pre-stress, it was decided to use an active material. Flexinol SMA wire was chosen since it can contract when heated and when it is cooled, it recovers back to its initial length. They have a great advantage of being widely available. Moreover, they can have a lifetime of millions of cycles, when used correctly. Both in the simulation and for the prototypes, Flexinol wire with a diameter of $0.375mm$ and a contraction strain of 4% was chosen.

The frame that holds the SMA wire and the flexures is made using additive manufacturing. The frame is made of PET-G using Fused Deposition Modelling (FDM) with a Prusa MK3S 3D-printer. PET-G was chosen because of its high operating temperature. Since the SMA wire in the center would be heated, it would not have an influence on the mechanical properties of the frame in case of PET-G. The distance from the center of the frame to the outer edge (length of the frame: l_{fr}) was one of the design parameters. The frames have four slits on each of the legs for the leaf springs and a hole in the center of the frame for the Flexinol wire.

The leaf spring flexures were dipped in superglue and inserted in the slits of the frame. The Flexinol wire was inserted through the holes in both frames and clamped at the outside of the frame using 2-pin wire joints. Figure 7 shows all the parts that are used to fabricate the joints and figure 8 shows a fabricated joint. It can be seen that extra flanges are added to the top and bottom frames. These are used to clamp the joints machine during the experiments.

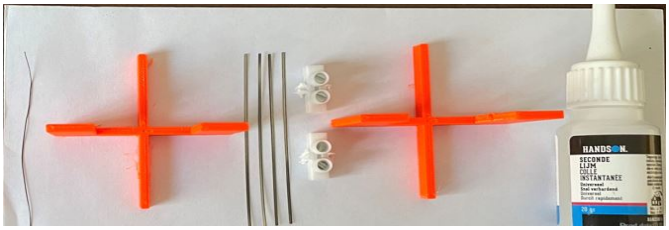

Fig. 7. All the parts used for fabrication. From left to right: Flexinol wire, frame, leaf spring flexures, wire joint connectors, frame and superglue.

E. Material Properties

The joint is made of three different components: a PET-G frame, Leaf Spring flexures and a Flexinol SMA wire. The two frames are 3D-printed, with leaf springs in between them, that act as flexures, see figure 8. In the centre of the joint, there is a Flexinol SMA wire that contracts when it is heated. The 3D-printed frames are made of PET-G, which has a Young's modulus of 2100 MPa and shear modulus of 1375 MPa.

The leaf springs are made of EN1.4310 steel. The Young's Modulus for this steel can vary depending on the supplier. For the simulation of the CANS-J, a Young's Modulus of 210 GPa and a shear modulus of 80 GPa is used.

The SMA wire in the centre is a Flexinol wire, that is made of a nickel-titanium alloy. The Flexinol has the unique behavior that it contracts when it is heated. Depending on how much current is applied, the wire has a contraction strain of 3 - 5 %. SMA wires are highly sensitive to heat. When overheated, their mechanical properties will change and this will influence

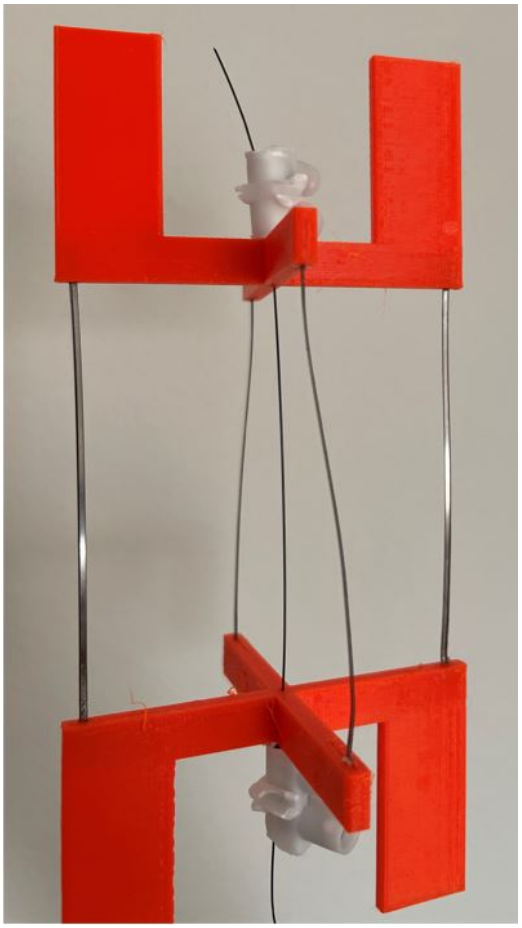

Fig. 8. The fabricated joint.

the reversible behavior. SMA wires have 2 different Young's moduli since they have two different phases: martensite and austenite. The reported Young's modulus for the wires is 28 GPa and 75 GPa for martensite and austenite, respectively. When the Flexinol wire is heated, it contracts. This happens because the SMA wire goes from the martensitic state to an austenitic state [15],[16]. In the neutrally stable state, the Flexinol wire is thus in the austenite phase. Therefore, Young's modulus of the austenite phase is used for the simulation in the activated state and Young's modulus of the martensite phase is used for the simulation in the non-activated state. For the shear modulus, 28.2 GPa and 10.5 GPa is used for austenite and martensite, respectively.

F. Test setup

Each of the five fabricated samples was tested in both the neutrally stable (activated) state and the stiff (non-activated) state. Experiments on the joints were done using a ZwickRoell Z005 torsion machine.

The experiments in the activated state were done as following: each of the five samples was placed in the torsion machine and clamped at the bottom frame. Once the joint was clamped at the bottom frame, a current was applied for one second using a 9V battery making the Flexinol wire and the joint contract. The joint was then clamped at the top frame. The current could not be continuously applied, because it would overheat the Flexinol wire, thereby changing the material properties of it. The torsion machine then applies a rotation to the top frame. However, the rotation angle in the experiments was 5 to 15 degrees smaller than the angle θ', used in the simulation. This is done to prevent the samples from breaking. Thereafter, the sample is rotated in the opposite direction twice the angle initially applied. Finally, it is then rotated back to its initial position. This whole process of rotations is repeated three times for every sample.

The experiments in the inactive state were done as following: each of the five samples was placed in the torsion machine and clamped at both the bottom frame and the top frame, without applying current to the Flexinol wire. A similar process of rotations as during the experiments in the active state was then applied.

In both experiments (active and inactive state), torque was measured at the bottom frame of the joint, using the HBM T20WN torque sensor. This resulted in torque-angle graphs which can be seen in section III.

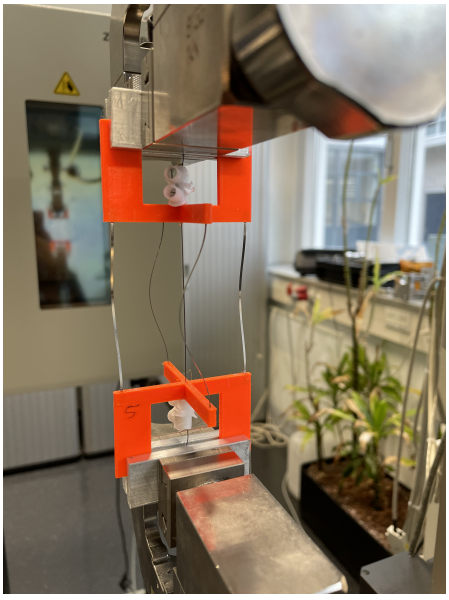

Fig. 9. The joint clamped inside the torsion machine.

III. Results

Figure 10 shows the torque-angle graphs of the geometries that showed behavior which is close to neutrally stable from the simulations. The torque-angle graphs from the experiments of these 5 geometries can also be seen in figure 10. It can be seen that in the simulation the five geometries show a flat range, where the torque required for rotation is close to zero. The slope of the curve in the flat region is not completely zero, but slightly increasing. Thus, the joints have positive stiffness in the simulation. In the experiment graphs, it can be seen that apart from sample 3, all other samples show behavior which

is close to bi-stable behavior. This means that the joints are stiffer in the simulation than in reality.

In the experiment graph of all the samples, there is a region where the torque required to rotate is close to zero. Moreover, it must also be noted that there is some noise visible in the trough and peak of the torque-angle graph from the experiments of sample 4 and 5, respectively. This is due to the change of buckling direction of the leaf springs during rotation.

In can be seen that the neutral stablility range is similar in both the simulation and the experiments. Table III shows the the neutral stability ranges of the both the simulation and the experiments for the five samples.

Neutral Stability Range

Sample	Simulation	Experiments
1	25	22
2	34	33
3	45	44
4	50	45
5	65	50

TABLE III
NEUTRAL STABILITY RANGE OF THE 5 GEOMETRIES IN DEGREES.

In figure 11, the simulation and experiments results of the 5 samples in the non-activated can be seen. It should be noted that in the simulation, sample 4 and 5 are stiffer than in the experiments. In the experiments graphs, there is a range where sample 4 and 5 seem to be neutrally stable.

Figure 12 gives the results of the experiments of the the 5 samples in both the non-activated state and the activated state. All 5 samples are tested 3 times in both states. It can be seen that, in the non-activated state, all the five samples still have a range where the torque required to rotate is zero. However, this range is much smaller compared to the activated state. Furthermore, it can be seen that in both states, there is hysteresis in the experiments.

IV. DISCUSSION

A. *Effects of Parameters*

From the results of the simulation and the experiments, it can be seen that the neutral stability range increases with the height in both the simulation and the results. This is to be expected when looking at the theoretical model of rotation in equation 4. When the height of the joint increases, it should be able to rotate more. However, when the height increases, the stiffness of the leaf spring flexures also decreases. These two factors explain the increasing neutral stability range with the increasing height.

The fives geometries that follow from the simulation do show neutrally stable behavior in the activated state, however their stiffness in the non-activated state is very low. In figure 12, it can be seen that in the non-activated state, the samples can be rotated without the application of much torque. The

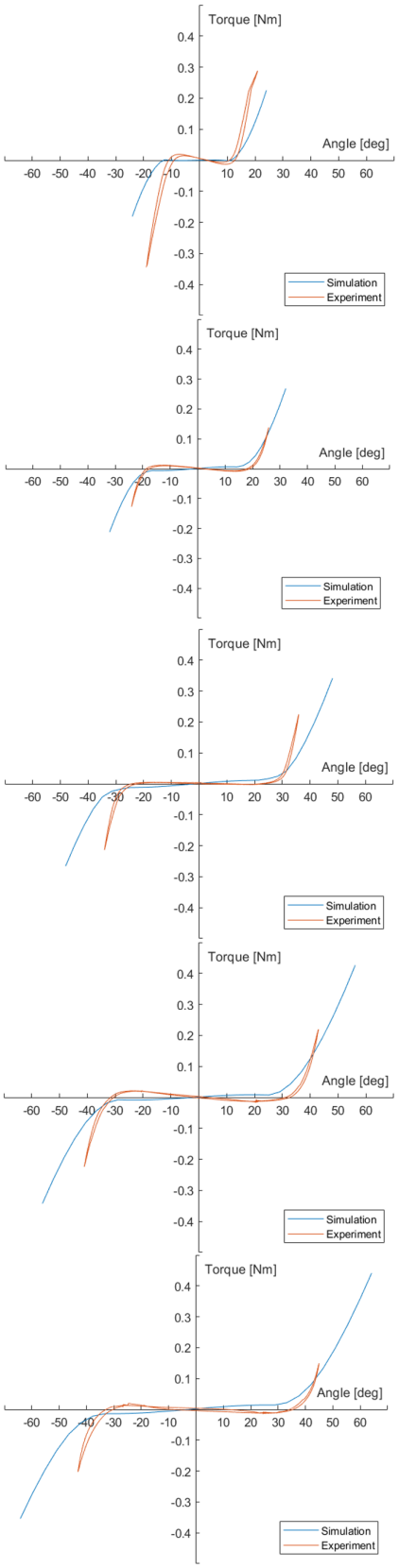

Fig. 10. Simulation and experiments results of the activated state. Top to bottom: Sample 1 through 5.

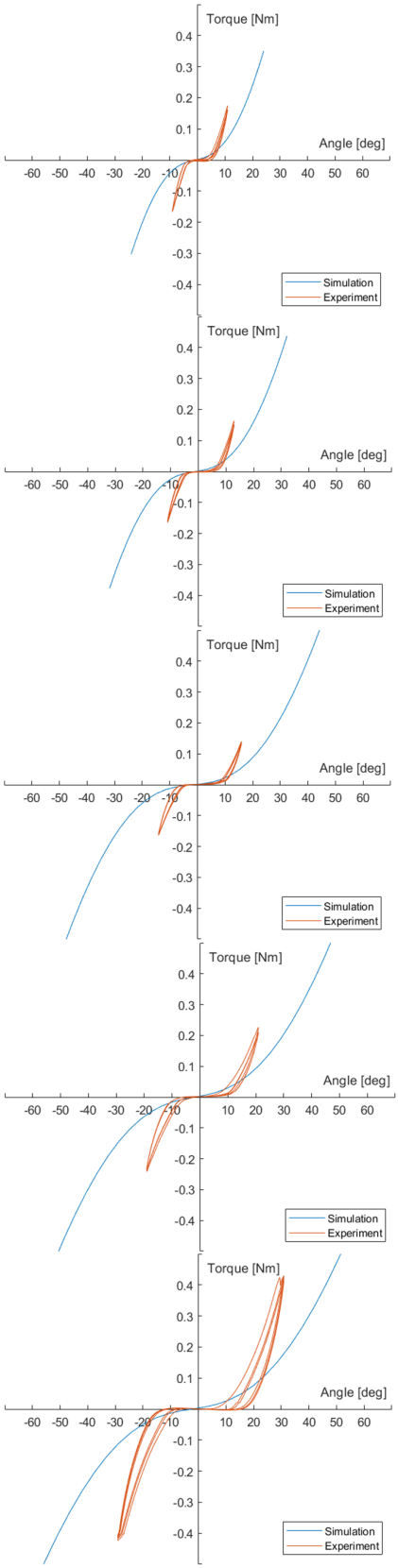

Fig. 11. Simulation and experiments results of the non-activated state. Top to bottom: Sample 1 through 5.

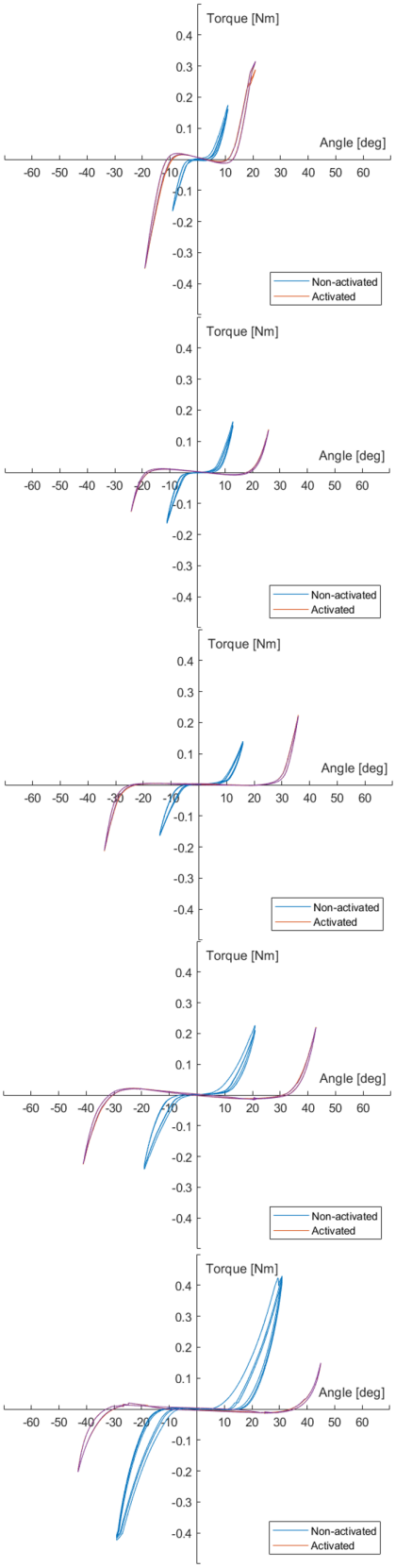

Fig. 12. Experiments: Non-activated vs activated state. Top to bottom: Sample 1 through 5. Each sample is tested 3 times in both states.

samples seem to have a neutral stability range in the non-activated state as well. This is because the dimensions of flexures that follow from the simulations are small. The reason for this is that the Flexinol wire that is used is thin. It can therefore not exert much force. If the joint is to be made stiffer in the non-activated state, the width and the thickness of the leaf springs should be increased. However, a thicker Flexinol wire should be then used as well. This will also increase the off-axis stiffness of the joint.

B. Comparison of Simulation with Experiments

Comparing the results from the simulation with the results from the experiments, it can be seen that the neutral stability ranges of the five samples in the experiments are a bit smaller than the ranges in the simulations. The differences are very small and could be explained by inaccuracy in the fabrication method. The leaf spring flexures are, as explained before, lasercut. The leaf springs have a low thickness and width. This has the consequence that, once these flexures are lasercut and separated, they are slightly bent, making them a bit stiffer then they would be if they were completely straight. Therefore, when the whole joint is made using these bent leaf spring flexures, it has a higher stiffness in reality than in the simulation. This leads to a smaller neutral stability range in the experiments than in the simulation.

There is also a difference in the constraints applied in the simulation and the experiments. In the simulation, the constraints are applied at the center of the frames, whereas in the experiments, the whole frame is clamped and restricted from movement. Furthermore, in the simulation, the top frame can freely move up and down, whereas in the experiments the top frame can not move once it is activated and clamped, adding extra stiffness to the joint. This may also result in a lower neutrally stable range.

This extra added stiffness due to the clamping of the top frame is expected to have more influence in the non-activated state than in the activated state. In the activated state, the leaf springs are buckled, when the sample is clamped. This means that the sample can be rotated easily. In the non-activated state, the leaf springs are unbuckled (stiff), making it more difficult to rotate. Thus, this also means that the neutrally stable ranges visible in the non-activated state in figure 12 are smaller then they would be if the experiments were done without clamping the top frame of the sample.

The positive stiffness in the simulation graph of the activated state, figure 10, may be due to overestimation of the Young's modulus of the steel leaf springs. The Young's modulus of the specific steel used can vary from 190 to 210 GPa. In the experiments, the samples show bi-stable behavior. This means, that the steel leaf springs may in reality be less stiffer than in the simulation.

All the five samples show hysteresis. The frames of the joint are made of PET-G which shows visco-elastic behavior when it is loaded [17]. This means that energy is dissipated when the a PET-G part is loaded and unloaded. Hysteresis could be decreased by making the frames stiffer.

Another interesting difference between the simulation and the experiments is the difference in the applied rotation angle. In the simulation, an angle of $1.5 \cdot \theta$ is applied to rotate the joint, whereas in the experiments this angle could not applied. Therefore, a smaller angle is used to rotate during the experiments. This can be explained by the fact that the simulation does not check for plastic deformation, whereas in reality if the angle applied is too high, the joint would deform plastically.

C. Further research

In order to minimize the difference between the simulation and the experiments, the samples could be made using a monolithic method of fabrication. This would decrease the inaccuracy errors in the fabricated sample. Furthermore, more samples for each set of geometry could be made and tested multiple times, instead of testing one sample of each geometry 3 times.

Moreover, the movement constraints at the top frame in the experiments could be made similar to the constraints in the simulation. This could be done by sending short impulses of currents through the Flexinol wire. This way, the wire would not overheat and the top frame would not need to be clamped completely. The top frame would then only experience rotation, similar to the simulation.

When looking at the results, the neutrally stable range could be increased by making the joint higher or stacking multiple joints on top of each other. This has the problem, that the higher the joint gets, the more compliant it gets. The stiffness can be increased by changing the dimensions of the leaf spring flexures and using a thicker Flexinol wire. This way the off-axis stiffness wil also be higher.

The results of this paper, in general provide opportunities for activatable neutrally stable compliant mechanisms. Active materials combined with certain movement constraints can act as pre-stress to make neutrally stable compliant mechanisms switch between the stiff state and the neutrally state.

D. Real-life applications

The main goal of this research is to research the possibilities of making neutrally stable compliant mechanisms switch between the stiff state and a neutrally stable state. The results of this research can however also be used for real-life applications.

It can be used in applications where certain mechanisms are only allowed to open when something is detected. For example, a door that can only be opened if the right password is inserted. When the right password is inserted, a signal is sent to a current source which applies a current on the Flexinol wire, making the joint neutrally stable and thus opening the door.

Satellites circulating around the world use solar panels to generate electricity. However, when these satellites are being transported to the their location, these solar panels are folded and when they reach their location, the solar panels are unfolded. In order to fold and unfold, a joint is required that

can switch between a stiff and a neutrally stable state. The CANS-J could be used for this purpose.

The CANS-J can also be used as a joint where only a specific amount of rotation is required. The simulation can be optimized to find dimensions corresponding to the desired range of motion.

V. Conclusion

In this paper, a new Compliant Activatable Neutrally Stable Joint (CANS-J) is presented. The main advantage of this joint is that it can switch between a stiff state and a neutrally stable state by turning on and off the pre-stress, unlike previous neutrally stable compliant joints. Furthermore, since the joint is only exposed to stress when it is required, it also tackles the problem of creep in compliant mechanisms. The joint is made using 3D-printed PET-G frames that hold leaf spring flexures and a Flexinol wire. The Flexinol wire can be activated to contract, which provides the stress for the leaf springs flexures to buckle. The design is simulated and a grid search is done to determine which combination of design parameters give the desired behavior. From the simulations five geometries followed that showed neutrally stable behavior. These five geometries are fabricated and tested. A clear neutrally stable range is visible in the experiments, which goes from 22 degrees for the smallest sample to 50 degrees for the largest sample. These ranges of motion correspond the simulation. This means that simulation can be used to find different set of parameters of the joint to achieve the desired range of motion.

The thin Flexinol wire has the consequence that the dimension of the CANS-J are as such, that it has a low off-axis stiffness. However, upon further developments, the CANS-J can be used as an application in mechanisms that need to open and close. In general, CANS-J shows that active materials have a great potential as a provider of stress in neutrally stable compliant mechanisms.

Acknowledgment

The authors would like to thank the staff at the PME lab for their cooperation and help during the fabrication and the experiments phase.

References

[1] Larry L. Howell. “Introduction to Compliant Mechanisms”. In: *Handbook of Compliant Mechanisms*. John Wiley & Sons, Ltd, 2013. Chap. 1, pp. 1–13. ISBN: 9781118516485. DOI: https://doi.org/10.1002/9781118516485.ch1.

[2] Mark Schenk and Simon D Guest. “On zero stiffness”. In: *Proceedings of the Institution of Mechanical Engineers, Part C: Journal of Mechanical Engineering Science* 228.10 (2014), pp. 1701–1714.

[3] Chia-Wen Hou and Chao-Chieh Lan. “Functional joint mechanisms with constant-torque outputs”. In: *Mechanism and Machine Theory* 62 (2013), pp. 166–181. ISSN: 0094-114X. DOI: https://doi.org/10.1016/j.mechmachtheory.2012.12.002. URL: https://www.sciencedirect.com/science/article/pii/S0094114X12002303.

[4] Chao-Chieh Lan and Jung-Yuan Wang. “Design of adjustable constant-force forceps for robot-assisted surgical manipulation”. In: *2011 IEEE International Conference on Robotics and Automation*. 2011, pp. 386–391. DOI: 10.1109/ICRA.2011.5979556.

[5] Pietro Bilancia et al. “Zero Torque Compliant Mechanisms Employing Pre-Buckled Beams”. In: *Journal of Mechanical Design* 142 (Apr. 2020), pp. 1–14. DOI: 10.1115/1.4046810.

[6] Ishit Gandhi and Hong Zhou. “Synthesizing constant torque compliant mechanisms using precompressed beams”. In: *Journal of Mechanical Design* 141.1 (2019).

[7] Christine Jutte, Sridhar Kota, and Robert Dennis. “Closed-Loop Tape Springs as Fully Compliant Mechanisms: Preliminary Investigations”. In: (Jan. 2004). DOI: 10.1115/DETC2004-57403.

[8] Thanh-Vu Phan, Huy-Tuan Pham, and Cong-Nam Truong. “Design and Analysis of a Compliant Constant-Torque Mechanism for Rehabilitation Devices”. In: Jan. 2020, pp. 541–549. ISBN: 978-3-030-45119-6. DOI: 10.1007/978-3-030-45120-2_44.

[9] Joshua Allen Crews. *Methodology for analysis of stress, creep, and fatigue behavior of compliant mechanisms*. Missouri University of Science and Technology, 2016.

[10] Sebastiaan Joosten, Giuseppe Radaelli, and Heike Vallery. “Passive autonomy: hygromorphic rotational actuators”. In: *Smart Materials and Structures* (Nov. 2020). DOI: 10.1088/1361-665x/abcf1e. URL: https://doi.org/10.1088/1361-665x/abcf1e.

[11] Mel Schwartz. *Smart materials*. CRC press, 2008.

[12] Jaronie Mohd Jani et al. “A review of shape memory alloy research, applications and opportunities”. In: *Materials & Design (1980-2015)* 56 (2014), pp. 1078–1113. ISSN: 0261-3069. DOI: https://doi.org/10.1016/j.matdes.2013.11.084. URL: https://www.sciencedirect.com/science/article/pii/S0261306913011345.

[13] Jean-Marc Battini. “Co-Rotational Beam Elements in Instability Problems”. In: (May 2002).

[14] O. A. Bauchau and J. I. Craig. “Euler-Bernoulli beam theory”. In: *Structural Analysis*. Ed. by O. A. Bauchau and J. I. Craig. Dordrecht: Springer Netherlands, 2009, pp. 173–221. ISBN: 978-90-481-2516-6. DOI: 10.1007/978-90-481-2516-6_5. URL: https://doi.org/10.1007/978-90-481-2516-6_5.

[15] J. Van Humbeeck. “Shape Memory Alloys: A Material and a Technology”. In: *Advanced Engineering Materials* 3.11 (2001), pp. 837–850. DOI: https://doi.org/10.

1002/1527-2648(200111)3:11⟨837::AID-ADEM837⟩3.0.CO;2-0.

[16] Dieter Stöckel. “The shape memory effect - Phenomenon, alloys, applications”. In: *Proceedings of Shape Memory Alloys for Power Systems* (Jan. 2000).

[17] Yun Luo, Luc Chevalier, and Eric Monteiro. “Basis for viscoelastic modelling of polyethylene terephthalate (PET) near Tg with parameter identification from multi-axial elongation experiments”. In: *International Journal of Material Forming* 7 (Sept. 2014). DOI: 10.1007/s12289-013-1129-8.

Appendices

A

Design, Prototyping and Fabrication

The design of the CANS-joint is inspired by the HRA [7]. In the HRA, the movement along the centerline and the top and bottom edges of the actuator is restricted. Thus, when the wooden sheet is elongated, the HRA shows rotational behavior. However, during the initial prototyping phase, a similar yet opposite design was thought of. Instead of applying the movement constraint to the centerline, constraint are applied to the outer side edges along with the constraint on the top and bottom edges. And instead of elongating the wooden sheet, the sheet is compressed. The two designs can be seen in figure A.1. The red lines show where the constrains are applied, i.e. where the movement of the device is restricted. The arrows show the movement (strain) direction.

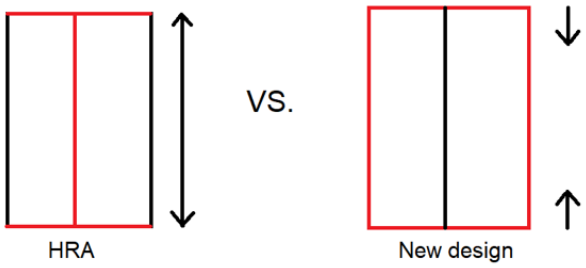

Figure A.1: The 2 different designs. The black arrows show the strain direction (expansion vs. contraction). The red lines show where the motion is restricted.

First prototypes were made to test the two proposed designs, which can be seen in figure D.1. These prototypes are made of polymorph, which is a material that can be shaped in any form when it is heated. If it is then cooled, it will keep the shape, until heated again.

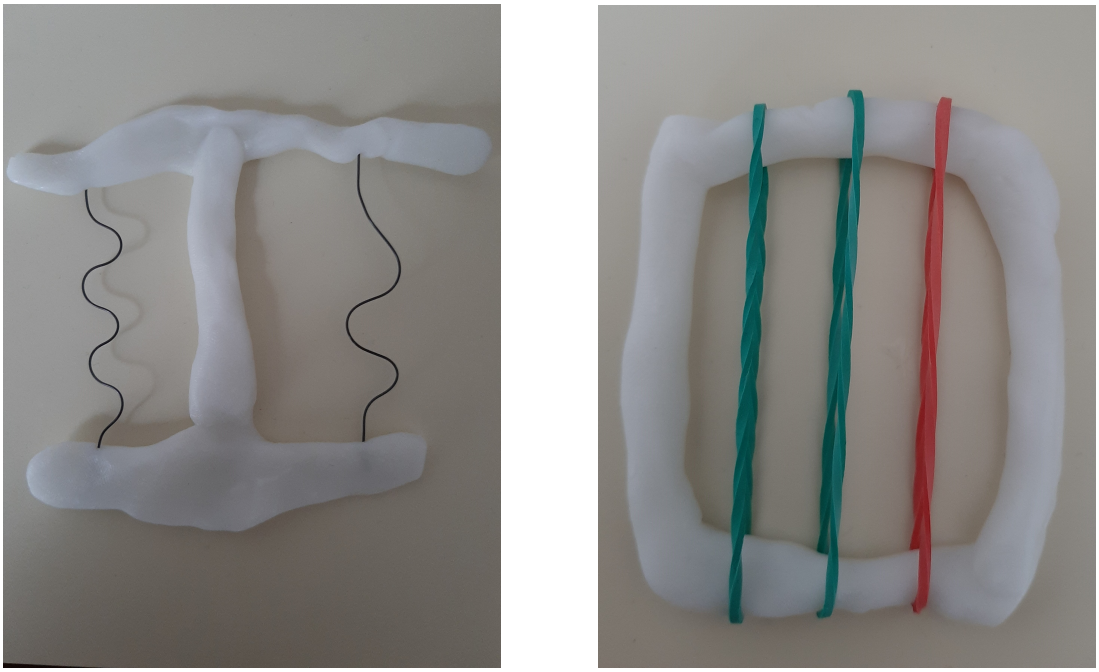

Figure A.2: Prototypes of the 2 designs

After considering both designs, it was decided to develop and continue the new design, where the movement constraints are applied on the outer edges and the device contracts in the centre. This had two reasons. First: from literature, it was discovered that materials that shrink are much more easily available. Secondly, the prototypes of the new design, showed a very clear bi-stable behavior. This meant, that there had to be some dimensions, where it would show neutrally stable behavior.

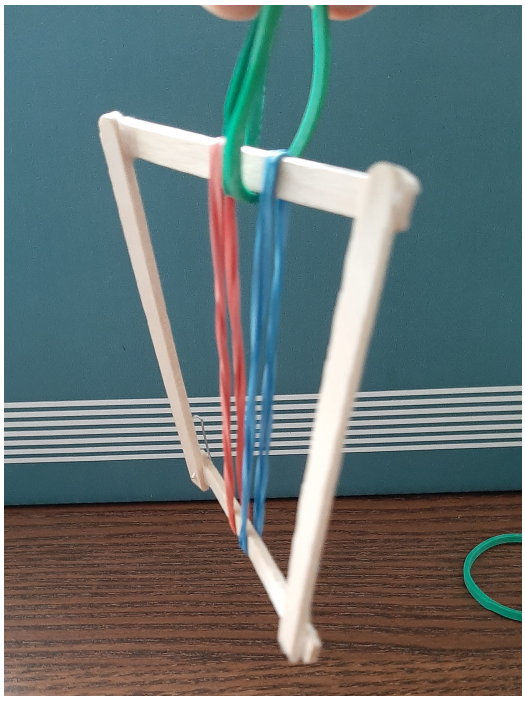

Figure A.3: Wooden prototype of the new design

In figure A.3 above, a more advanced prototype of the new proposed design can be seen. It is made of four small wooden sticks attached to each other and 2 elastic rubber bands, that provide the stress.

This stress could be adjusted by adding or removing rubber bands. This way, the bi-stable - and till some extent - the neutrally behavior could be made visible.

A.1. Materials

Analysing the new design, it can be divided in three different parts: a top and bottom frame, flexures that are held in place by these frames and something that shrinks and this provides the stress in the center of the joint.

Since the main purpose of this thesis is to turn on and off the stress, the choice for active materials was made. Active (or smart) materials are materials that can respond to external stimuli and thereby change their physical properties in response [11]. From literature, it was found that a Shape Memory Alloy (SMA) wire could be used for this purpose. SMA wires can react to heat stimuli and thereby change their physical appearance [9]. Since the active material needed for the previously discussed design should contract and thereby provide stress, Flexinol SMA wire was chosen. A Flexinol wire is a type of SMA wire that specifically contracts with a strain of 4% when it is heated. When it is cooled, it will elongate back to its initial length [13],[12]. If the heating of the Flexinol wire is done correctly, it will have a lifetime of millions of cycles. Flexinol wire with a diameter of $0.375mm$ was chosen.

A commonly used part in compliant mechanisms as flexures are leaf springs. These leaf springs can deflect efficiently, and thus corresponding to the property that compliant mechanisms move by using the deflections of its members. The leaf springs are made of EN1.4310 steel and were laser cut with varying dimensions, which followed from the simulation. These leaf springs were cut using Optec microlaser cutter with a 15 Watt Talon UV nanosecond pulsed laser.

The frames that holds the leaf springs and the Flexinol wire together were 3D-printed using PET-G with a Prusa MK3S 3D-printer. PET-G was chosen instead of the more common PLA 3D-printing material, because PET-G has a higher operating temperature than PLA. Since the Flexinol wire would be heated, it would also heat the frame. It is therefore desired that this heat does not influence the physical/mechanical properties of the frame material. Thus, a material with higher operating temperature was selected.

The proposed design was simulated in Matlab using the materials described here-above to determine which set of parameters would give the desired neutrally stable behavior, see appendix C. The mechanical properties of the materials used in the simulation are given in table A.1.

	PET-G	EN1.4310 Steel	Flexinol
Young's Modulus	2.1 GPa	210 GPa	75 GPa
Shear Modulus	1.375 GPa	80 GPa	28.2 GPa

Table A.1: Mechanical properties of the materials used in the simulation

A.2. Fabrication

From the simulation, 5 geometries followed which showed neutrally stable behavior. These 5 samples were fabricated using the materials described above.

As stated in the previous section, frames were 3D printed using PET-G which would hold the leaf spring flexures and the Flexinol wires. For each sample, 2 frames were 3D-printed. These frames have slits in them for the flexures and a hole in the centre that goes through the whole frame for the Flexinol wire, see figure A.5. The top and bottom of the leaf springs were dipped in superglue and were inserted in the slits of the frames on either side of the flexures. Once all the 4 flexures were in both the frames, the whole joint was let to dry. After 15 minutes, the Flexinol wire was inserted through the holes in both frames. Initially, the wire was held in place using metal glue. However, when the wire was heated, the metal glue was also influenced by the heat. Therefore, it was decided to use a mechanical clamp to hold the Flexinol wire in place. The mechanical clamp used was a 2-pin wire joint connector.

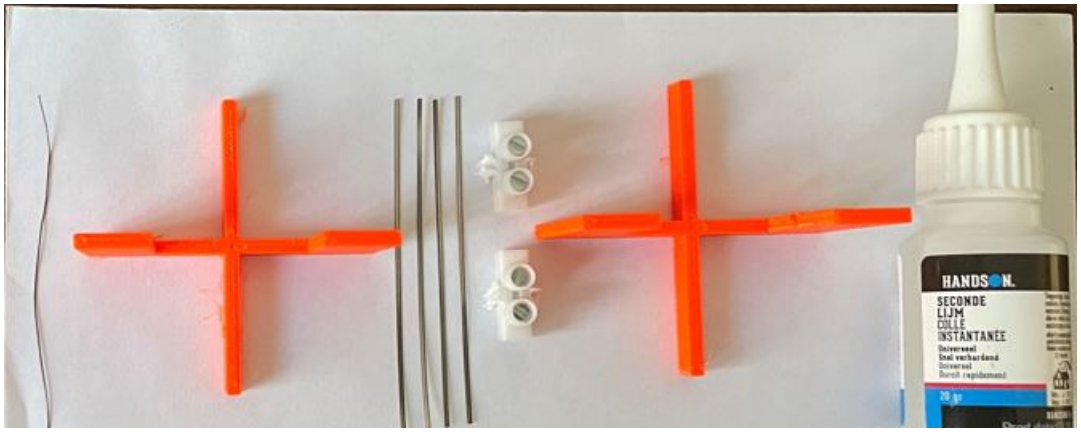

Figure A.4: All the parts used to fabricate the joint.

Figure A.5: Slits for the leaf spring flexures and the whole through which the SMA wire is inserted.

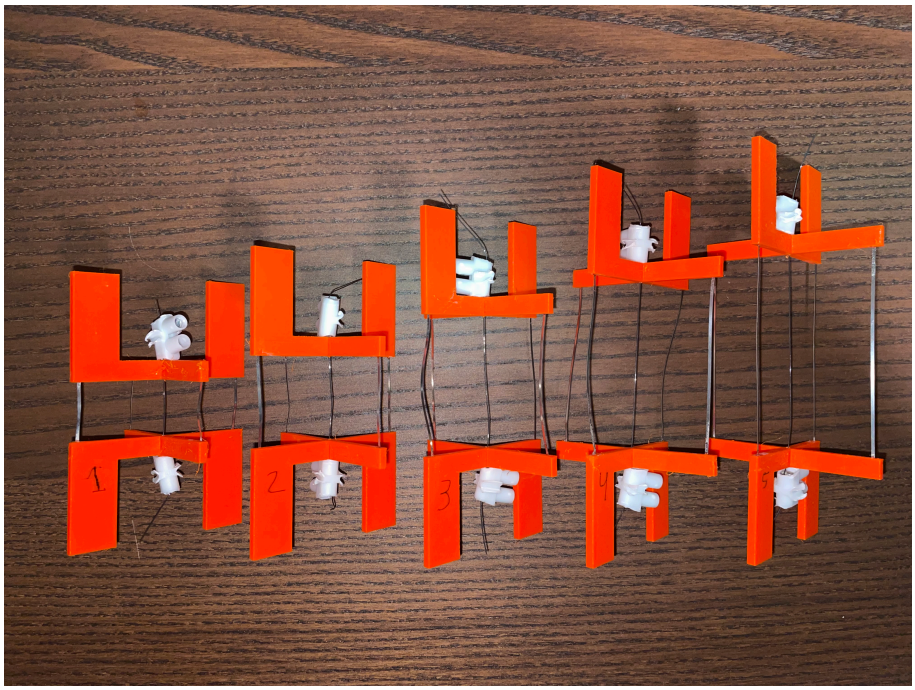

Figure A.6: The 5 fabricated samples

B

Theoretical Rotation

Since the CANS-J will show rotational behavior when it is activated, it can be calculated, how much this rotation will be. The rotational behavior of the CANS-J is similar to that of the HRA. Joosten, Radaelli, and Vallery have derived a model with which the theoretical rotation of the HRA can be calculated [7]. This model needs to be slightly adjusted for it to be valid for CANS-J. This is due to the fact that the constraints are applied on different locations and the strain direction is opposite. First, the model derived in [7] for the HRA is explained. Then in the second section, it is explained what adjustments have been made and how the new model looks like.

B.1. Model for the HRA

In [7], the authors have derived a model that gives the theoretical possible rotation of the HRA when it is in the activated state. The basis of this model is as follows: in the deformed state, the HRA will take on a shape that resembles a helicoid. This helicoid shape can be projected onto a cylindrical surface. When this surface is unfolded, a triangular shape will be formed, see figure B.1. Each side of the unfolded triangle can be related to a geometrical parameter of the HRA, i.e., h gives the height of the HRA along the center and L gives the length of the outer edges of the HRA. The length of the outer edges, L, is driven by the expansion strain of the material, S_h and the height, h. Therefore, this length, L, can be defined as follows:

$$L = h \cdot (1 + S_h) \tag{B.1}$$

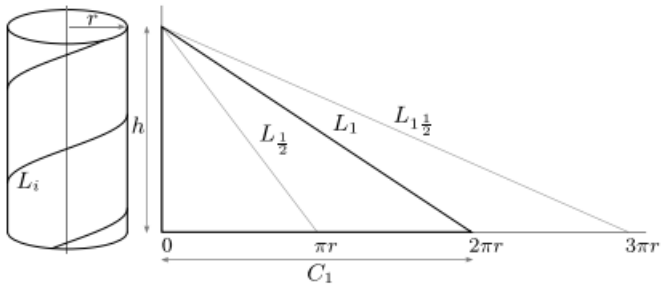

Figure B.1: Figure from [7]

When looking at figure B.1, the length, L, can also be defined as follows:

$$L = \sqrt{h^2 + C^2} = \sqrt{h^2 + (2\pi)^2 \cdot r^2} \tag{B.2}$$

Substituting equations B.2 and B.1 and solving for 2π gives the following equation for the theoretical possible rotation in the activated state:

$$2\pi = \sqrt{\frac{(h \cdot (1 + S_h))^2 - h^2}{r^2}} \tag{B.3}$$

This equation can then be further worked out and rewritten to get the rotation angle in degrees:

$$\theta = \frac{180}{\pi} \sqrt{(S_h^2 + 2S_h)\frac{h^2}{r^2}} \tag{B.4}$$

B.2. Model for the CANS-J

The model explained in the previous section is valid when the helicoid shape is obtained by way of expansion. However, in the case of CANS-J, the helicoid shape is obtained by way of contraction. Therefore, one assumption need to be adjusted.

Contrary to the model of the HRA, in CANS-J, the height, h, along the centre is driven by the length of the outer edges, L. In CANS-J, the length of the outer edges stays the same and the height along the centre changes with contraction strain. This is due to a slightly different working principle, as explained in Appendix A. The height, h, can therefore be defined as follows:

$$h = L \cdot (1 - S_h) \tag{B.5}$$

Similarly, using figure B.1, the height, h, can then be defined as follows:

$$h = \sqrt{L^2 - C^2} = \sqrt{L^2 - (2\pi)^2 \cdot r^2} \tag{B.6}$$

Substituting equations B.6 in B.5 and solving for 2π gives the following equation for the theoretical possible rotation in the activated state:

$$2\pi = \sqrt{\frac{(L \cdot (1 - S_h))^2 - L^2}{r^2}} \tag{B.7}$$

This equation can then be further worked out and rewritten to get the rotation angle in degrees:

$$\theta = \frac{180}{\pi} \sqrt{(2S_h - S_h^2)\frac{L^2}{r^2}} \tag{B.8}$$

Replacing the parameters in this equation with parameters that describe the design of the CANS-J, gives the following equation:

$$\theta = \frac{180}{\pi} \sqrt{(2S_h - S_h^2)\frac{lf^2}{lfr^2}} \tag{B.9}$$

As it can be seen in the model, the theoretical rotation depends only on the height and the width of the joint.

C

Simulation

Before the final design was fabricated, simulations were done to get the optimal dimensions. These dimensions would give the largest neutral stability range. The CANS-J was modeled in Matlab using beam model based on the work of Battini, [2].

The whole joint was modeled in Matlab by defining nodes along the entire geometry where these node are connected to each other. Every element connecting two nodes is modeled as a beam of the Linear Beam Theory. The number of nodes can be increased, and thus increasing the number of elements used to define the geometry. More elements would give a more accurate result.

In this appendix, it is explained how the geometry is built and where and how the forces and constraints are applied. Before the code can be built, it is important to define a coordinate system. In figure C.1, the coordinate system used to build the code can be seen. Moreover, it should be clear that in essence the whole joint is made of 12 beams connected to each other with a 13^{th} beam representing the Flexinol wire.

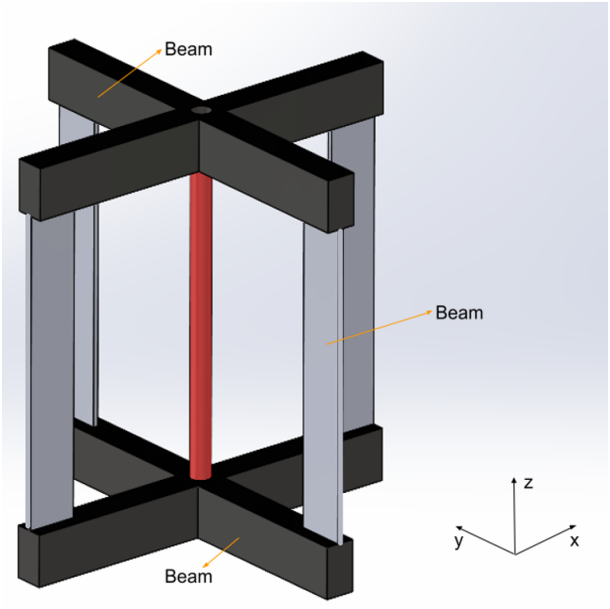

Figure C.1: Coordinate system used to build the code

C.1. Dimensions

At the beginning of the code, the dimensions corresponding to the geometry are added. It must be noted, that some of the dimensions are constant, whilst 4 dimensions are design parameters. It can

be seen in the following code that 3 of these 4 parameters (wf, tf & lfr) are used in for loops in combination with the try,catch function of Matlab. The fourth parameter (lf) is changed manually. Thus, for each value of lf, 3 for loops were run, in which the other three design paramters were varied.

```
%% Dimensions

d = 0.375e-3;   %diameter of the SMA wire in m
r = d/2;        %radius of the SMA wire

lf = 0.08;      %height of the flexures in m varied --> [0.03 0.04 0.05
    0.06 0.07 0.08]

tfr = 0.003;    %thickness of the cross shaped frame in m
hfr = 0.005;    %height of the cross shaped frame in m



    for wf = 0.001:0.001:0.005 %width of the flexures

        for tf = 0.0001:0.0001:0.0003 %thickness of the flexures

            for lfr = 0.01:0.005:0.030 %length of the frame --> the width
                of the joint

            try
```

C.2. Rotation

With this code, the theoretical possible rotation is calculated, using equation B.6. It is important to note that a scaling factor with the value of 1.5 is used to increase this rotation angle. This is because for some combination of dimensions, the angle calculated by equation B.6 was too small to show any movement.

```
%% Rotation

%This is the theoretical possible rotation; this equation is derived from
%the equation by Sebastiaan. According to this equation, the thickness and
%the width of the leaf flexures have no effect on the rotation.

theta = sqrt((lf^2/lfr^2)*0.0784);  %theoretical possible rotation
sf = 1.5;                           %scaling factor
thetasf = sf*theta;                 %scaled rotaion

rot1 = thetasf;                     %first rotation
rot2 = -2*thetasf;                  %second rotation
```

C.3. Elements

With this code, the geometry is split in as many as elements as required. First, the number of elements that should be used are given. Thereafter, each of 12 beams of the joint is divided in as many elements as given.

```
%% How many elements?

elms=10;                %number of elements, needs to be > 0
steps=elms+1;           %steps needed to create these elements


```

```
%% Settting up the vectors

x_y_bot = linspace(0,lfr,steps)';                %the length of the leg of
    the bottom cross frame in and x and y direction
x_top = linspace(0,lfr,steps)';                  %the length of the leg of
    the top cross frame in x direction

offset = zeros(steps,1);                         %the offset needed for the
     simulation to run
offset(end) = 0.000001;                          %offset

y_top = linspace(0.000001,lfr,steps)';           %the length of the leg of
    the top cross frame in y direction with the offset
y_top_neg = linspace(0.000001,-lfr,steps)';      %the length of the leg of
    the top cross frame in the negative y direction with the offset
vert = linspace(lfr,lfr,steps)';                 %this holds the x and y
    coordinates of the flexures, needed to plot the flexure at the end of
    the cross frame

nulv = linspace(0,0,steps)';                     %zero vector

z_r = linspace(0,lf,steps)';                     %length of the flexures
z_v = linspace(lf,lf,steps)';                    %height of the system
```

C.4. Defining the nodes along the geometry

In the following piece of code, each of the 12 beams is placed at the right placed and connected to the right beams.

```
%% Model
% generation of coordinates and connectivities

Mat1=[x_y_bot          nulv              nulv;          %Beam created
    in the x direction at the bottom of the crossframe
      vert             nulv              z_r;           %Flexure
         created the y = 0 plane, location = +lfr on the x-axis
      flip(x_top)      offset            z_v;           %Beam created
         in the x direction at the top of the crossframe
      -x_top           flip(offset)      z_v;           %Beam created
         in the -x direction at the top of the crossframe
      -vert            nulv              flip(z_r);     %Flexure
         created the y = 0 plane, location = -lfr on the x-axis
      flip(-x_y_bot)   nulv              nulv;          %Beam created
         in the -x direction at the bottom of the crossframe
      nulv             -x_y_bot          nulv;          %Beam created
         in the -y direction at the bottom of the crossframe
      nulv             -vert             z_r;           %Flexure
         created the x = 0 plane, location = -lfr on the y-axis
      nulv             flip(y_top_neg)   z_v;           %Beam created
         in the -y direction at the top of the crossframe
      nulv             y_top             z_v;           %Beam created
         in the +y direction at the top of the crossframe
      nulv             vert              flip(z_r);     %Flexure
         created the x = 0 plane, location = +lfr on the y-axis
      nulv             flip(x_y_bot)     nulv];         %Beam created
         in the y direction at the bottom of the crossframe
```

```
17
18 Mat2 = [Mat1 zeros(size(Mat1))]; %total matrix created, rotations added
19
20
21 Mattot = unique(Mat2,'rows','stable'); %removes repeated rows i.e.
       repeated nodes
22
23 %Some nodes are added because they are used multiple times, i.e. the
       origin
24 %and the top node
25 add = [0 0         0  0 0 0;
26        0 0         0  0 0 0;
27        0 0.000001 lf 0 0 0;
28        0 0.000001 lf 0 0 0];
29
30 Mattot = insertrows(Mattot, add, [6*elms length(Mattot) 9*elms-1 length(
       Mattot)+1]);
```

C.5. Connecting the nodes

Once the nodes are defined along the geometry, they need to be connected to each other. With the following code, each is node connected the node before. This connection is modeled as a beam element of the Linear Beam Theory.

```
1 %% The nodes are connected to each other
2
3 link = zeros(12*elms,2);    %zero matrix created to link the nodes: 12*
      elms are the beams of the frame+flexures
4
5 N = length(link);
6
7 %the nodes are linked with each other
8
9 for i=1:N+1
10
11     link(i,:) = [i i+1];
12
13 end
```

C.6. Physical and Mechanical Properties

In the following pieces of code, the physical and mechanical properties of the joint are applied to the corresponding beams.

```
1 %% Dimensions of the beams
2
3 B = ones(1,length(link));          %width
4 H = ones(1,length(link));          %height
5
6 B = tfr*B;                         %width of the frame
7 H = hfr*H;                         %height of the fram
8
9
10 B((elms+1):(2*elms)) = wf;                  %width of the flexures
11 B((4*elms+1):(5*elms)) = wf;                %width of the flexures
12 B((7*elms+1):(8*elms)) = wf;                %width of the flexures
13 B((10*elms+1):(11*elms)) = wf;              %width of the flexures
```

```
B(end) = d;                                    %width of the SMA

H((elms+1):(2*elms)) = tf;                     %height of the flexures
H((4*elms+1):(5*elms)) = tf;                   %height of the flexures
H((7*elms+1):(8*elms)) = tf;                   %height of the flexures
H((10*elms+1):(11*elms)) = tf;                 %height of the flexures
H(end) = d;                                    %height of the sma
```

```
%% Mechanical properties of the beams

m_beams.E                                  = 2.1e9 * ones(1,m_beams.
    numberElements);        %Young's Modulus of the frame
m_beams.E((elms+1):(2*elms))               = 210e9;
                                             %Young's Modulus of the flexure
m_beams.E((4*elms+1):(5*elms))             = 210e9;
                                             %Young's Modulus of the flexure
m_beams.E((7*elms+1):(8*elms))             = 210e9;
                                             %Young's Modulus of the flexure
m_beams.E((10*elms+1):(11*elms))           = 210e9;
                                             %Young's Modulus of the flexure
m_beams.E(end)                             = 75e9;
                                              %Young's Modulus of the SMA
    Wire

m_beams.G                                  = 1.375e9 * ones(1,m_beams.
    numberElements);       %Shear modulus of the frame
m_beams.G((elms+1):(2*elms))               = 80e9;
                                              %Shear Modulus of the flexure
m_beams.G((4*elms+1):(5*elms))             = 80e9;
                                              %Shear Modulus of the flexure
m_beams.G((7*elms+1):(8*elms))             = 80e9;
                                              %Shear Modulus of the flexure
m_beams.G((10*elms+1):(11*elms))           = 80e9;
                                              %Shear Modulus of the flexure
m_beams.G(end)                             = 28.2e9;
                                              %Shear Modulus of the SMA Wire


m_beams.A          = breedte.*hoogte;                                    %
    Surface area of the beams
m_beams.Iyy        = hoogte.*breedte.^3/12;                              %
    Moment of inertia
m_beams.Izz        = breedte.*hoogte.^3/12;                              %
    Moment of inertia
m_beams.J          = (breedte.*hoogte/12).*(breedte.^2+hoogte.^2);       %
    Moment of inertia


m_beams.A(end)       =  pi*(r^2);                                        %
    Surface area of the SMA wire
m_beams.Iyy(end)     = (pi*(r^4))/4;                                     %Moment
     of inertia of the SMA wire
m_beams.Izz(end)     = (pi*(r^4))/4;                                     %Moment
     of inertia of the SMA wire
m_beams.J(end)       = (pi*(r^4))/2;                                     %Moment
     of inertia of the SMA wire
```

C.7. Contraction of the SMA wire

This piece of code simulates the contraction of the Flexinol wire. In the simulation for the non-activated state, the strain is 0.

```
%% Contraction of the SMA wire

m_beams.prestrain      = zeros(1,m_beams.numberElements);
m_beams.prestrain([end]) = -0.04;
m_beams.prestrain_incremental = 'Yes';
```

C.8. Boundary conditions

In the following code, all the boundary conditions are applied. The nodes where the movement constraints, forces and movements are applied are listen in line 7 of the code. In line 8, the values corresponding to these boundary conditions are given.

In the simulation of the non-activated state, an extra constraint is added in line 7, which is $(12 * elms + 2) * 6 - 3$. The corresponding value for the constraint is 0 in line 8. This prevents the top frame from moving up and down. Thus, it simulates a fixed support, together with the other constraints.

Two nodes are repeated in this geometry, since they are connected to many different beams. The origin node is defined three times and the centre node of the top frame is also defined three times. Therefore, it is desired that all the nodes that are used multiple times do the same thing, i.e., the whole geometry acts as one. For this purpose, with the code from line 14 untill 19, it is made sure that all the origin nodes do the same thing and all the nodes defining the centre of the top frame do the same thing.

```
%% BOUNDARY CONDITIONS on begin- and endpoint

PreFe                  = zeros(m_beams.eqn,1);  %Preload
Fe                     = zeros(m_beams.eqn,1);


bc          = [1:6  (12*elms+2)*6-5 (12*elms+2)*6-4 (12*elms+2)*6];     % On which DOF's are there constraints? E.g.: 1:6 are the DOF's of the first node; 19 = the x coordinate of the 4th node, etc.
dofs.dp     = [0 0 0 0 0 0    0 0 rot1]';    %What is the value of the constraints applied hereabove?
dofs.all    = (1:m_beams.eqn)';
dofs.bc     = bc(~isnan([dofs.dp]));
dofs.dp     = dofs.dp(~isnan([dofs.dp]));
dofs.R      = sparse(1:length(dofs.bc),[dofs.bc],1+0*dofs.bc,length(dofs.bc),m_beams.eqn);

nieuwdeel = sparse([1:6 1:6 7:12 7:12 13:18 13:18 19:24 19:24],[1:6 (6*elms+1)*6-5:(6*elms+1)*6 1:6 (12*elms+1)*6-5:(12*elms+1)*6  (12*elms+2)*6-5:(12*elms+2)*6 (3*elms+1)*6-5:(3*elms+1)*6  (12*elms+2)*6-5:(12*elms+2)*6 (9*elms+1)*6-5:(9*elms+1)*6],[1 1 1 1 1 1 -1 -1 -1 -1 -1 -1 1 1 1 1 1 1 -1 -1 -1 -1 -1 -1  1 1 1 1 1 1 -1 -1 -1 -1 -1 -1  1 1 1 1 1 1 -1 -1 -1 -1 -1 -1],24,m_beams.eqn);
nieuwdeel2 = zeros(24,1);


dofs.R      = [dofs.R;nieuwdeel];
dofs.dp     = [dofs.dp;nieuwdeel2];
```

D

Test setup

In this chapter, the test setup is explained which was used to validate results from the simulation.

The ZwickRoell Z005 torsion machine was used to apply rotation and a HBM T20WN torque sensor was used to measure the resulting reaction torque. 2 experiments were done on each of the 5 samples. 1 experiment was in the activated state and the other was in the non-activated state.

The experiments in the activated state were done as follows. Each of the five samples was clamped in the torsion machine at the bottom frame. Once clamped in the torsion machine, a current was applied on the Flexinol wire for 1 second, making the wire and thus the joint, contract. The top frame was then clamped. Once the joint was clamped at both the top and the bottom frame in the torsion machine, the current is removed. Applying a current to the Flexinol wire for longer than a few seconds would overheat the wire. This would change the micro structure and thus the behavior of the wire.

A rotation was then applied on the sample. The scaled angle θ' from the simulation could not be applied in the experiments, because that angle would break the samples. The torque would reach the limit of the torque sensor, before the rotation angle was even reached. Therefore, the applied angle was 5 to 15 degrees smaller than thae angle θ' used in the simulation. After the first rotation, the sample was then rotated back with twice the angle applied. In the last step, the sample was rotated back to its initial position. During this whole process, the reaction moment at the bottom frame was measured. This process was repeated three times.

The experiments in the non-activated state were done as follows. The joint was clamped at both the bottom and the top frames. No current was applied on the Flexinol SMA wire. A similar process of rotations was applied. During rotations, the reaction moment at the bottom frame was measured. This process was also repeated three times.

D.1. Improvement of the experiments

It is important to note that the height of the joint is constrained by the torsion test bench. In the simulation, the height is not constrained at all and the top frame can move freely up and down. Furthermore, constraining the top frame also adds extra stiffness to the joint.

Therefore, in order to improve the experiments, the top frame should not be clamped at all. In the activated state, the height of the frame should be only constrained by the Flexinol wire. In order to overcome heating of the wire, short pulses of current can be applied to the wire instead of a constant current. The top frame should be only subject to rotation in both the activated and the non-activated states.

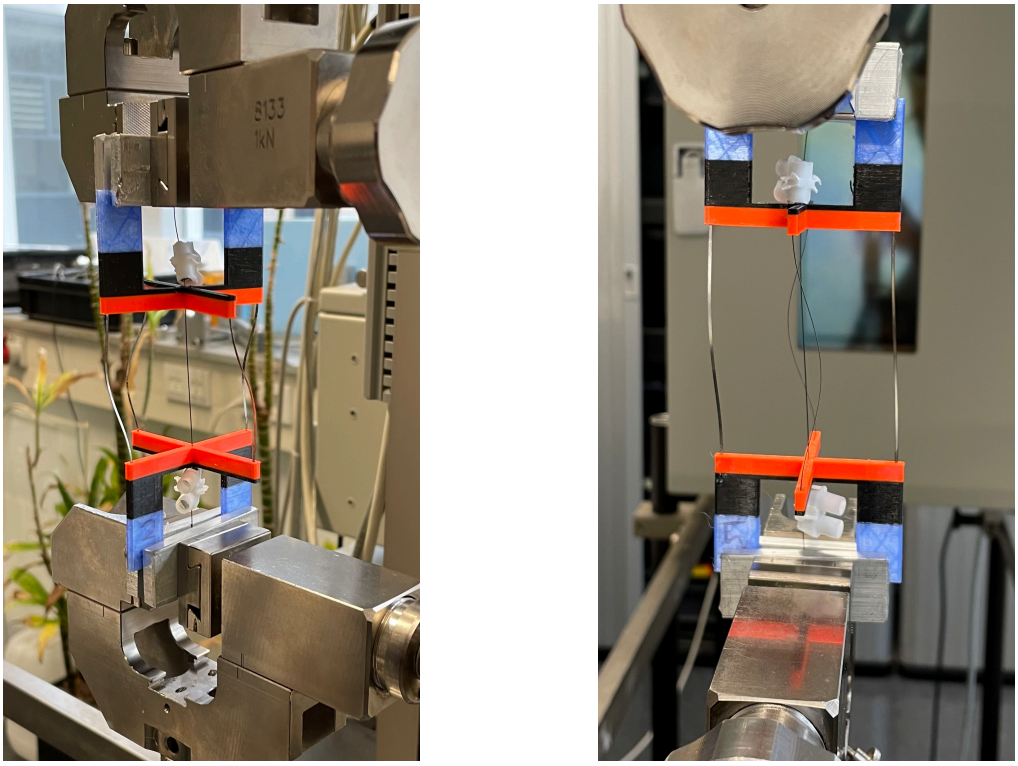

Figure D.1: Samples clamped in the test bench in the activated state.

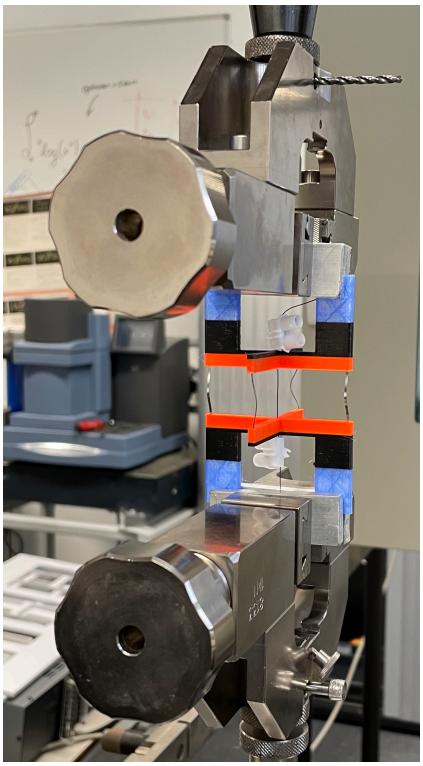

Figure D.2: Sample clamped in the test bench in the activated state.

Acknowledgements

I want to thank my supervisor Giuseppe Radaelli for his guidance and supervision during this thesis. Giuseppe, your guidance on the topic but also on a personal level is amazing. The past year has been one with many challenges. I cannot thank you enough for your understanding and helping me throughout the past year. I want to also thank Ali Amoozandeh Nobaveh for helping me with the code and giving me useful feedback during our meetings. Thank you to Professor Just Herder and Werner van de Sande for their feedback as the assessment committee.

Thank you to all the other students of this group, with whom I have worked together in the past year.

A special thanks goes out to my family. To my grandparents, who gave me all the love and the prayers of this world at a young age. To my parents, who gave me the freedom and supported me to follow my dreams. To my siblings, thank you for your unconditional support and for being a listening ear. To all the other family members, thank you for all the fruitful discussions and motivation. Without the prayers and support of my family, I would have never been able to achieve all of this. Thank you for always being there for me, in my highs and in my lows.

I would also like to thank my friends, that I have met in the past student years. It was not only about studying in Delft, it was also about making friends and memories. And I am glad to say that I have made wonderful friends and unforgettable memories that I will cherish all my life. I will miss our meetings at ”the balkon”, where we studied, where we had interesting discussions about everything, where we came up with so many business ideas. Who knows, one day we will work out that business idea and actually start our own company. And as odd as this may sound, I will most definitely miss our daily long train trips to and from Delft.

Bibliography

[1] *About Compliant Mechanisms*. URL: https://www.compliantmechanisms.byu.edu/about-compliant-mechanisms.

[2] Jean-Marc Battini. “Co-Rotational Beam Elements in Instability Problems”. In: (May 2002).

[3] Pietro Bilancia et al. “Zero Torque Compliant Mechanisms Employing Pre-Buckled Beams”. In: *Journal of Mechanical Design* 142 (Apr. 2020), pp. 1–14. DOI: 10.1115/1.4046810.

[4] Joshua Allen Crews. *Methodology for analysis of stress, creep, and fatigue behavior of compliant mechanisms*. Missouri University of Science and Technology, 2016.

[5] Ishit Gandhi and Hong Zhou. “Synthesizing constant torque compliant mechanisms using pre-compressed beams”. In: *Journal of Mechanical Design* 141.1 (2019).

[6] Larry L. Howell. “Introduction to Compliant Mechanisms”. In: *Handbook of Compliant Mechanisms*. John Wiley & Sons, Ltd, 2013. Chap. 1, pp. 1–13. ISBN: 9781118516485. DOI: https://doi.org/10.1002/9781118516485.ch1. eprint: https://onlinelibrary.wiley.com/doi/pdf/10.1002/9781118516485.ch1. URL: https://onlinelibrary.wiley.com/doi/abs/10.1002/9781118516485.ch1.

[7] Sebastiaan Joosten, Giuseppe Radaelli, and Heike Vallery. “Passive autonomy: hygromorphic rotational actuators”. In: *Smart Materials and Structures* (Nov. 2020). DOI: 10.1088/1361-665x/abcf1e. URL: https://doi.org/10.1088/1361-665x/abcf1e.

[8] Christine Jutte, Sridhar Kota, and Robert Dennis. “Closed-Loop Tape Springs as Fully Compliant Mechanisms: Preliminary Investigations”. In: (Jan. 2004). DOI: 10.1115/DETC2004-57403.

[9] Jaronie Mohd Jani et al. “A review of shape memory alloy research, applications and opportunities”. In: *Materials & Design (1980-2015)* 56 (2014), pp. 1078–1113. ISSN: 0261-3069. DOI: https://doi.org/10.1016/j.matdes.2013.11.084. URL: https://www.sciencedirect.com/science/article/pii/S0261306913011345.

[10] Mark Schenk and Simon D Guest. “On zero stiffness”. In: *Proceedings of the Institution of Mechanical Engineers, Part C: Journal of Mechanical Engineering Science* 228.10 (2014), pp. 1701–1714. DOI: 10.1177/0954406213511903. eprint: https://doi.org/10.1177/0954406213511903. URL: https://doi.org/10.1177/0954406213511903.

[11] Mel Schwartz. *Smart materials*. CRC press, 2008.

[12] Dieter Stöckel. “The shape memory effect - Phenomenon, alloys, applications”. In: *Proceedings of Shape Memory Alloys for Power Systems* (Jan. 2000).

[13] J. Van Humbeeck. “Shape Memory Alloys: A Material and a Technology”. In: *Advanced Engineering Materials* 3.11 (2001), pp. 837–850. DOI: https://doi.org/10.1002/1527-2648(200111)3:11<837::AID-ADEM837>3.0.CO;2-0.

II

Literature Review

1

Literature Review: Responsive materials with high expansion caused by an external stimulus

Delft University of Technology

Literature Review

Responsive materials with high expansion caused by an external stimulus

Author:
Hanzalah Ahmad (4567471)

Supervisor:
Giuseppe Radaelli

21-01-2021

Abstract

Zero-stiffness structures require no external work to change and maintain their position. Smart or active materials are materials that can deform when an external stimulus is applied. In this review, different smart materials are researched for the use in a zero-stiffness joint using the working principle of the Hygromorphic Rotational Actuator. In order to achieve zero-stiffness in a structure, pre-stress is required. This stress can be caused by smart materials in the active state, when their deformation is constrained. An overview is presented of different smart materials with their corresponding stimulus and the properties of these materials such as the response time and strain. The found materials are graded in a performance criteria on their properties to determine which material is of the best use.

Contents

Chapter 1 Introduction

Compliant mechanisms are mechanisms that use the flexibility of their members to elastically deform and generate motion, rather than using separate stiff and rigid parts with hinges [8]. Compliant mechanisms therefore require less parts, have high precision due to less wear and backlash, and can be easily used in MEMS devices [1],[8]. An interesting compliant mechanism to make is a zero-stiffness joint.

A zero-stiffness device can deform and then stay in the deformed state, without the application of any force or moment [26]. However, achieving zero-stiffness in compliant mechanisms requires pre-stressing. The disadvantage with this, is that when the pres-stress is continuously applied, it can cause creep. This has a consequence that one is not able to switch between the stiff and zero-stiffness state. Therefore, it would be interesting if one is able to apply the pre-stress when the zero-stiffness state is desired and remove the pre-stress when the stiff state is desired. This can be done using smart materials.

Smart materials are materials that can change their properties when an external stimulus is applied [27]. These materials can for instance change their shape or color. Examples of stimuli are a change in temperature, pressure or pH-levels. Some smart materials even show reversible behavior, which means that the materials deform back to their original shape, when the stimulus is removed. Smart materials have applications in many fields including the medical, aerospace and civil engineering fields [27]. Banerjee et al. present a thermo-responsive hydrogel that has wound-healing properties [2]. Simiriotis et al. use Shape Memory Alloy (SMA) to design and control actuators which can change the geometry of the wing of an aircraft [28]. Zhu et al. have designed a hydrogel that is filled in cement which gives the cement self-healing properties in case of crack occurrence [39].

So in order to make a compliant zero-stiffness joint that can switch between the stiff and zero-stiffness state, a combination of smart material and pre-stress is required. This combination is used in an actuator which is found in “Passive autonomy: hygromorphic rotational actuators” [13]. The authors have developed an actuator made of wood that rotates when it is exposed to a humid environment. The rotation is caused by expansion of the material on the one hand and constraining the movement on the other hand. When the actuator is made wet, the sheet of wood tends to elongate in the z-direction. However, this movement is constrained along the z-axis, see figure 1.1. Furthermore, the top and bottom horizontal edges are constrained to a 90 degrees angle along the z-axis, see figure 1.1. As a consequence of these applied constraints, the total height is fixed. However, in order to accommodate for the length change, the wooden sheet will twist, causing the top of the actuator to rotate with respect to the bottom.

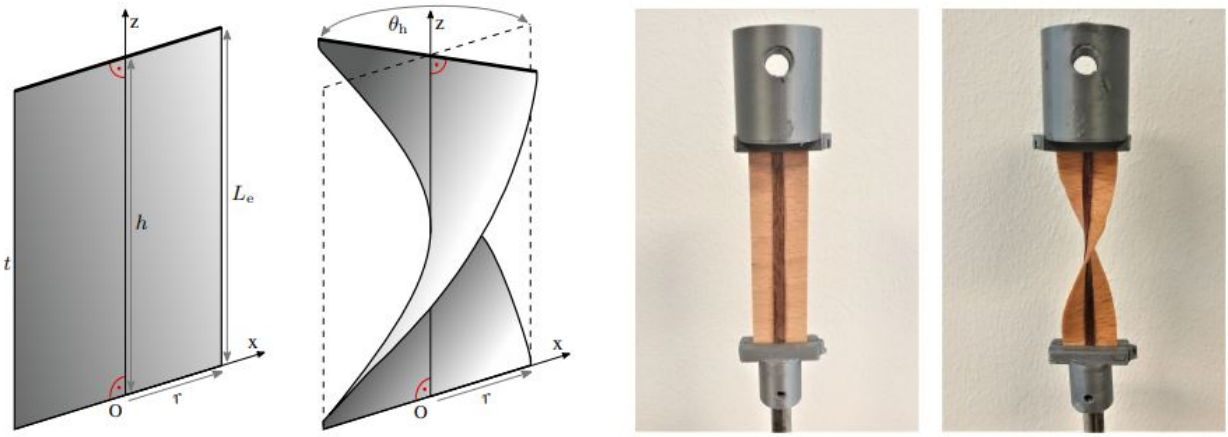

Figure 1.1: Schematic view of the actuator (left) and the actuator in non-activated and activated state (right) [13].

1.1 Problem

During the production of the actuator, the authors came across an interesting behavior when it is activated. The stress that causes the rotational behavior seems to also cause a behavior which is that the actuator has a range of angles over which it can rotate without any torque required. This is the already discussed zero-stiffness behavior. Figure 1.2 below shows the behavior of the actuator in the non-activated and activated state.

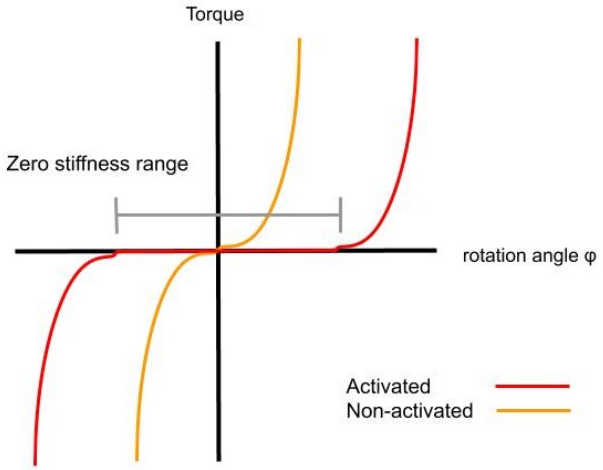

Figure 1.2: Zero stiffness range

The authors in [13] have thus made an actuator. However, the working principle of this actuator and the pre-stress caused by that working principle can be used to make a compliant zero-stiffness joint.

However, this device has some disadvantages in order to use it properly as a joint. First of all, the material which is used is wood, which makes the device fragile. This has a consequence that its applications are very limited. Furthermore, once the stimulus is taken away, the device does not fully deform back to its original shape. So, one can not completely switch between the stiff and the zero-stiffness state. It can also be only activated twice or thrice.

The objective of this report is therefore to find materials that elongate or shrink when an external stimulus is applied. Not only should these materials respond to a stimulus, the materials should also show reversible behavior. This means that when the stimulus is taken away, the material should deform back to its original shape.

1.2 Report structure

First, it will be explained how the papers for this literature study were found. Then, in chapter 3, the results of the found papers will be presented and categorized on properties that are of importance for this problem. In chapter 4, the results are graded on a performance criteria. Chapter 5 discusses the results of this review and chapter 6 ends the paper with conclusions.

Chapter 2 Search Method

In order to perform this literature study, SCOPUS and Google Scholar were used to find relevant papers. The terms that were used to find these papers are shown in the following table. The search terms in the rows were used with "OR" function with respect to the other rows and the columns were used with the "AND" function with respect to the other columns. This means that the search results must have at least one term of each column.

	AND			
OR	Smart Structures	Stimulus	Response	Elongation
	Smart Materials	Stimuli	Responsive	Expansion
	Shape memory polymers*	Stimuli-responsive	Multi-stimuli response	Bending
	Shape memory alloys*	Environmental-sensitive		Bilayer
	Smart structural systems	Mechanical stimulus		Shape changing
	Shape memory*	Chemical stimulus		Deformation
	Smart actuators			Shape morphing
	Shape changing polymers			
	Hydrogels			
	Reconfigurable metamaterials			
	Electroactive polymer			
	Intelligent actuators			

*: shape memory materials are materials that can recover their original shape under the influence of a specific stimulus [9].

All the papers used in this review are found in the way described above. During the search process, there were also papers giving smart materials which are used in the field of Civil Engineering or Biology. These papers are not used, since they could not be applied for the application proposed in this review.

Chapter 3 Literature Findings

In this chapter, the findings of the literature review will be presented. The results of all the papers found by the search method explained in chapter 2 will first be given one by one after which a table overview that lists the most important properties will be given.

Since we are looking for materials that deform to an external stimulus, the results are categorized by the external stimulus applied. The stimuli presented in this review are: thermal, light, electrical, water/humidity, pH-stimulus and chemical. Since the obtained papers only presented materials which are either polymers or metals, they are further categorized by these two materials.

3.1 Thermal

3.1.1 Polymers

Gao et al. have made a bilayer which is made of polyvinylidene fluoride (PVDF) and graphene oxide (GO) layers [6]. The bilayer is multi-responsive as it reacts to thermal, IR light and moisture stimulus. The bilayer can bend when it is heated up to 37 °C. This light will cause heat which results in volume expansion of the PVDF layer and volume contraction in the GO layer. Since the PVDF layer elongates and the GO layer shrinks, the bilayer will bend, see figure 3.1. When the stimulus is taken away, it returns back to the original shape, after which it can be used again. The strain of this actuator is 0.2 % for the thermal stimulus.

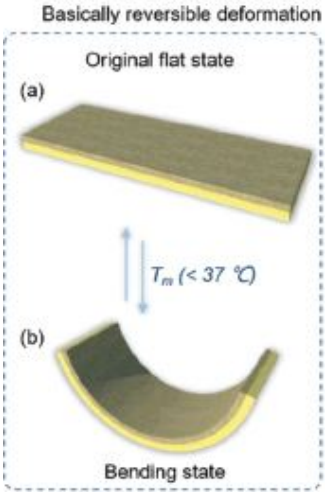

Figure 3.1: GO/PVDF bilayer [6]

Wang et al. have made a composite film which is made of polypyrrole nanoparticles (PPYNPs) added in a agar (AG) solution [33]. The use of PPYNPs makes this film multi-responsive. In this section, the thermal stimulus is presented. When the film is placed on a hot glass substrate, the beam bends upwards. This is due to the fact that the side of the film in contact with the glass substrate expands faster than the opposite side of the film. This difference is expansion causes the bending. The bending curvature can be increased by increasing the temperature. From the bending curvature, the strain is calculated to be 0.09 %.

Wang et al. have made a soft actuator that is made of SMP fibers in an elastomer matrix [30]. The matrix material is TangoPlus and the fibers are made of VeroClear. The actuator consists of the two layers. The top layer is the matrix material reinforced with the SMP fibers, whereas the bottom layer is made of only the matrix material. The fibers are reinforced with an angle. This means that the fibers are not parallel to the matrix material in the longitudinal direction, but they are inclined. This has a consequence that when the actuator is heated up, it deforms into a helical shape. The strain of this actuator is 13.5 %.

In [32], the authors have made a bilayer actuator, which consists of c-copolymer SMP layer on top of an elastomer layer (rubber). Before the SMP layer is attached on top of the rubber elastomer layer, it can be stretched upto a strain of 200 %. When the bilayer is heated upto 60 °C, the SMP layer shrinks back to its original shape. This decrease in length of one layer causes bending of the actuator. The response time is 30 seconds.

Rodriguez et al. [25] have made a semi-crystalline actuator that bends when it is heated upto 70 °C, see figure 3.2. The actuator is made of cross-linked ethylene vinyl acetate copolymer (cEVA) inside a polyester urethane elastomer (PU). The reported strain of this actuator is 30 % and can be used many times.

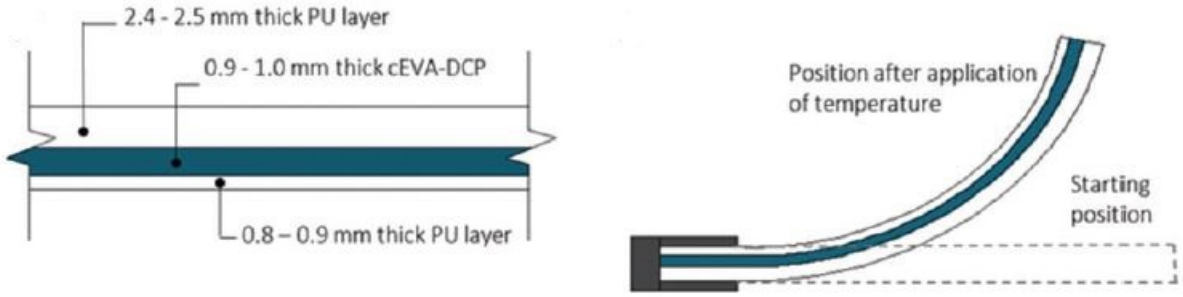

Figure 3.2: cEVA copolymer in PU elastomer [25]

Pringpromsuk, Xia, and Ni have made a multi-responsive actuator that responds to a heat stimulus [22]. It is made of shape memory polyurethane with dibutyl adipate (DBA) plasticizers incorporated in it. This forms a SMP gel. When this gel is heated, it can be deformed to a temporary fixed shape. When it is then further heated, it can return back to its original shape in 5 seconds, see figure 3.3. The authors decided deform the SMP gel into a temporary helical shape, however it can be deformed into any shape. When the stimulus is applied, the SMP gel will deform back to its original shape.

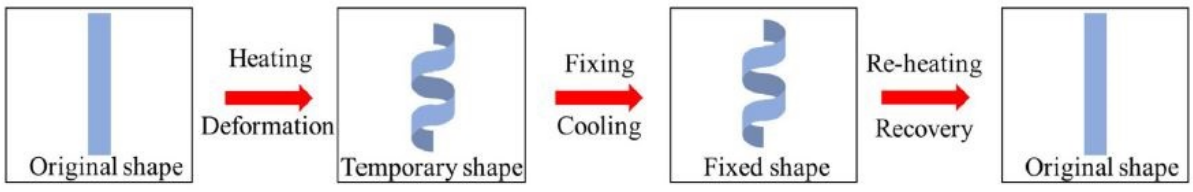

Figure 3.3: Multi-responsive actuator [22]

Wei et al. have made an actuator that is made of Nafion-Polypropylene-Polydimethylsiloxane (PDMS)/Graphite multilayers [35]. This actuator shows revesible behavior and responds to thermal, optical and humid stimuli, see figure 3.4 on the following page. This section explains the thermal stimulus. When the multilayer is heated up to 80 °C, the PDMS/Graphite layer will have a volume expansion, whereas the Nafion layer will shrink due to water disporption. This causes the the multilayer actuator to bend towards the Nafion layer in 31 seconds.

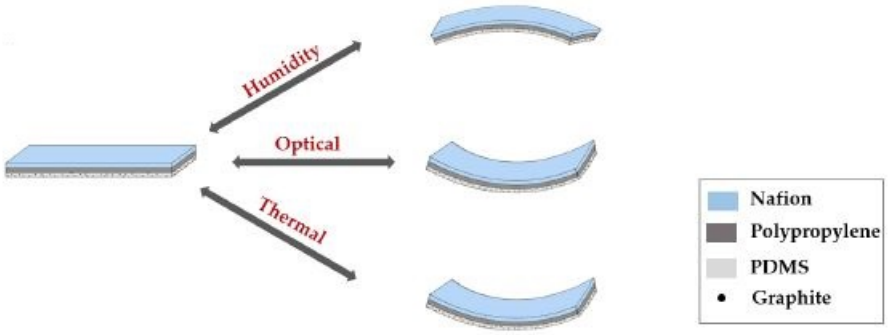

Figure 3.4: Multilayer actuator [35]

Liu et al. have developed a reversible hydrogel actuator that responds to a thermal stimulus. When the actuator is immersed in water of 50 °C, it bends, see figure 3.5. The calculated strain is 5 %. It is remarkable to note that water is also necessary for the actuator to work. However, the authors have decided to present it as thermal stimulus.

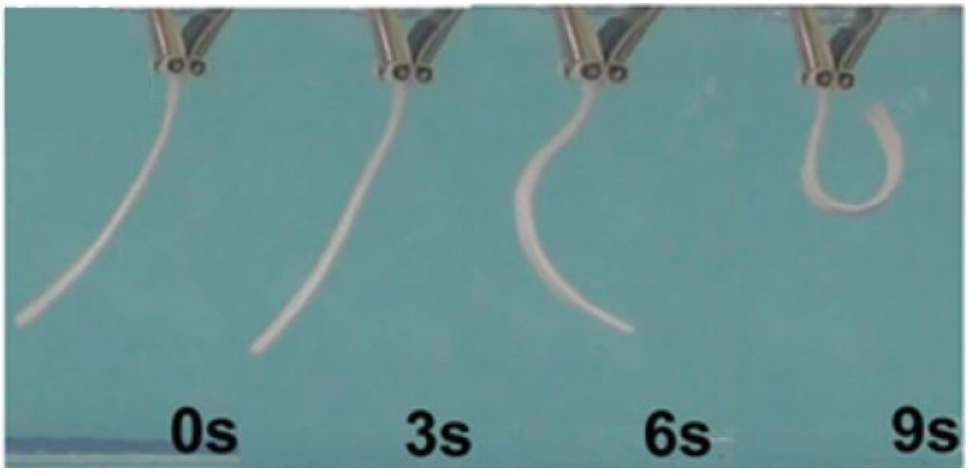

Figure 3.5: Hydrogel actuator [16]

He et al. have made a reversible bilayer hydrogel actuator that responds to thermal and NIR (near-infrared) stimuli [7]. This section presents the thermal stimulus. The actuator is made of polyNIPAM/GO hydrogel, however due to the distribution of the GO, it is transformed in a bilayer structure. Similar to the previous section, this actuator also bends when it is inserted in hot water, see figure 3.6.

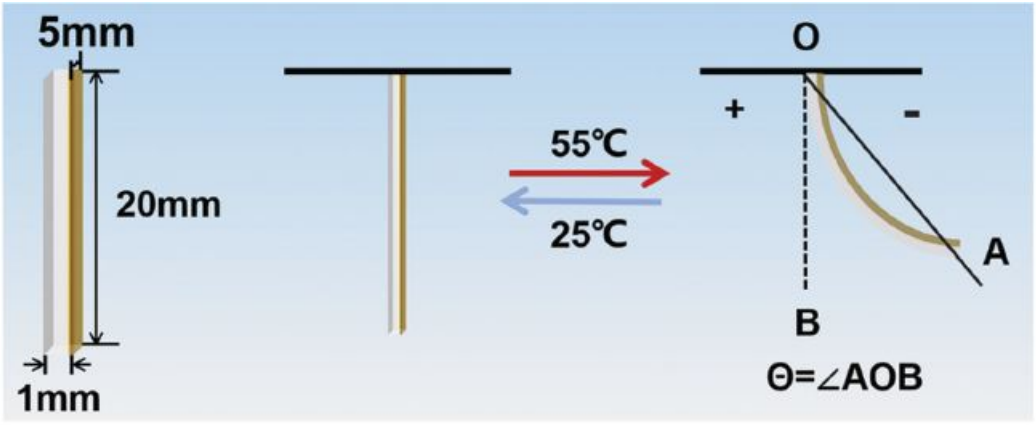

Figure 3.6: Hydrogel actuator [7]

3.1.2 Metals

Li, Huang, and Liu have made an actuator which is made of SMA wire in a silicon rubber matrix [15]. The SMA wire is deformed into a curved wire which is then embedded in a matrix material. When the temperature is increased to 340 K, the SMA wire inside the matrix will deform to straight shape. When this stimulus is taken away, the SMA wire will then deform back to a curved shape, see figure 3.7. In this case, the SMA wire is actuated by heating up the matrix with the SMA wire inserted in it. Later in section 3.3.2, more SMA wires are presented, which are actuated using electrical stimulus, i.e., letting a current go through the SMA wire.

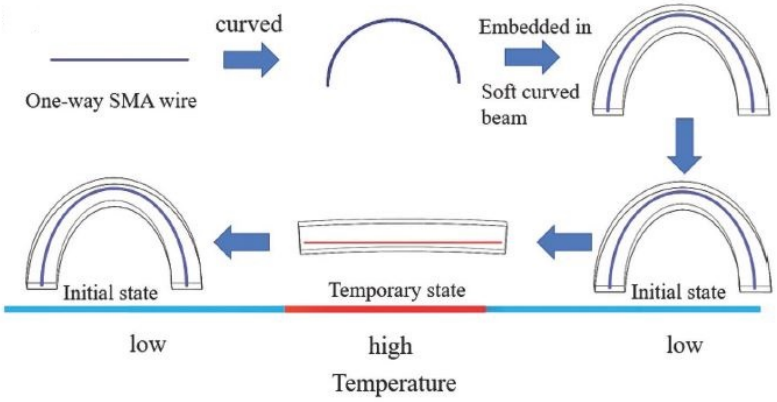

Figure 3.7: SMA wire in a matrix [15]

3.2 Light

As stated in section 3.1.1, Gao et al. have made a bilayer actuator of GO/PVDF layers, which responds to thermal, IR light and moisture stimulus. When the IR-light is applied, the actuator bends towards the GO side with a strain of 0.16 %. When the IR-light is removed, it deforms back to its original shape.

4d-printing is a way of manufacturing that uses 3d-printing and smart materials, which react to an external stimulus [20]. Jeong et al. use 4D-printing to develop a system that will deform when a specific light is applied [11]. The authors have made a sheet of a material called Tango+ that has two different types of digital shape memory polymer fibers - Veroyellow and Verocyan - inserted in it. Digital materials are created by 3D-printing multiple polymers with different properties to obtain a desired composite polymer [36]. When this sheet with the fibers is printed, it can be stretched with a strain of 10 % using heat treatment at a temperature of 90 degrees. If the fibers are then selectively heated up to a temperature T_g of 67 °C, the fibers will deform back, which cause bending. This selective heating is done via a light stimulus. If red LED illumination is applied, the light will only be absorbed by the Verocyan fibers, which heats up. As a consequence, the blue fibers will deform back to their original shape. Since the yellow fibers do not react, their shape stays the same. This difference in length in the fibers causes the bending, see figure 3.8. If it is then illuminated with blue light, it will deform back to the flat state. If the fibers are heat treated again, they can be used again.

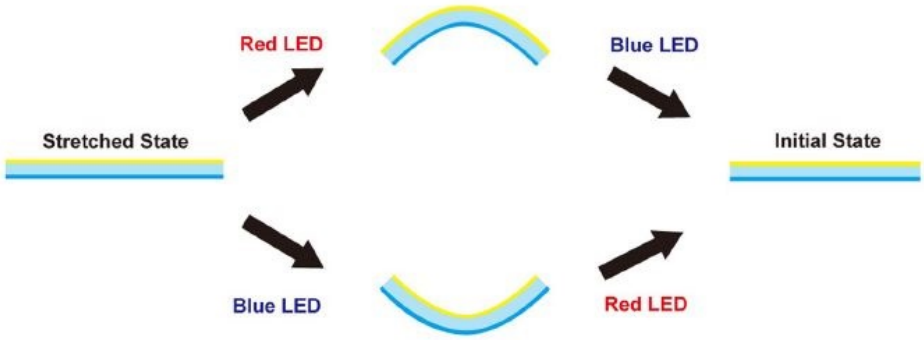

Figure 3.8: SMP fibers under light stimulus. [11]

As stated in section 3.1.1, Wang et al. have made a multi-stimuli actuator. One of these stimuli is light. When NIR light irradiation is applied to one side of the film, it absorbs light, which results is an increase in temperature and thermal expansion. This thermal expansion on side cause the beam to bend to the other side within 1 second. Increasing the light intensity, increases the bending curvature.

Pilz da Cunha et al. have made a bilayer actuator, which is bent in its initial state, that responds to light and a magnetic stimulus [21]. The bilayer actuator is made of a light responsive liquid crystal network (LCN) layer on top of a magnetic responsive polydimethylsiloxane (PDMS) composite layer, see figure 3.9. The light stimulus causes the bilayer to unbend, whereas with the magnetic stimulus the rotation can be controlled. It is remarkable to note that the initial shape of the bilayer is a bent shape.

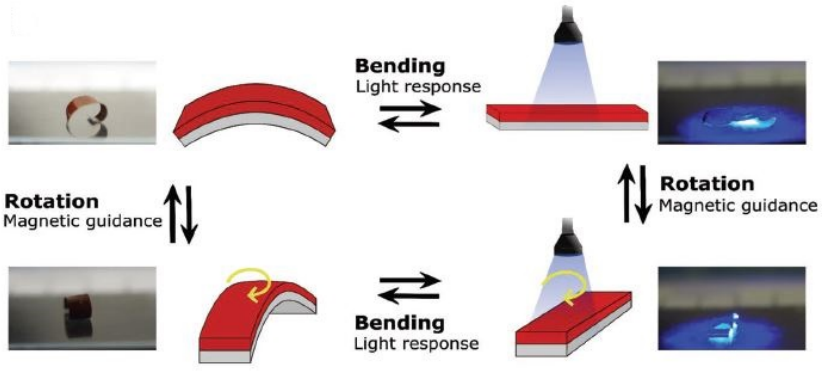

Figure 3.9: LCN/PDMS bilayer [21]

He et al. have made a bilayer hydrogel actuator. This actuator responds to thermal and NIR stimuli. This section explains the NIR stimulus. When the actuator is exposed to NIR light, it curls within in 17 seconds with a strain of 5.8 %.

Chen et al. have made a reversible bilayer actuator made of GO/PNIPAM hybrid films. When a near-infrared (NIR) light stimulus is applied, the bilayer shows bending behavior within 2 minutes. This is due to the shrinkage of the PNIPAM in the bilayer system when exposed to NIR light. The strain of this actuator is 2.75 %. When this stimulus is removed, the bilayer recovers its original shape in 20 minutes.

3.3 Electrical

3.3.1 Polymers

In [17], the authors have made an actuator which is made of ionogel graphene composite. This actuator reacts to an electric stimulus. The actuator reacts in 5 seconds and when the stimulus is removed, it deforms back to its initial shape. When the electric stimulus is applied, the ions in the ionogel will cause assymetric expansion, which leads to the bending deformation, see figure 3.10. Furthermore, if the polarity is inverted, the direction of bending can be changed.

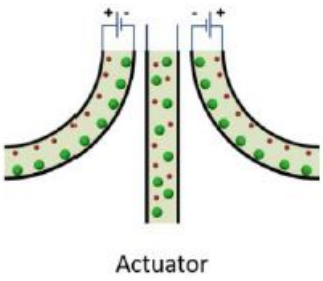

Figure 3.10: Ionogel graphene actuator [17]

Kim et al. have made a poly(methacrylic acid) (PMAAc) and sodium alginate (SA) hydrogel sheet that bends when an electric field is applied [14]. The working principle of this actuator is similar to the actuator explained previously. The direction of the bending is due to polarity of the applied electric field. The bending is thought to caused by the movement of the ions and the expansion of one side of the polymer and contraction of the other. It is important to note that before an electric stimulus is applied, the hydrogel sheet is immersed in a HCl solution to make it swell.

Jiang et al. also report a bending hydrogel sheet when an electric stimulus is applied. In this case, the author have used a Al-NC gel. The bending behavior is reversible. However, it can only be actuated for a limited number of 10 times.

3.3.2 Metals

The device explained in section 3.1.2 - SMA wire by Li, Huang, and Liu - can also be used in combination with an electrical stimulus [15]. Since this active material is a conductive wire, it can be connected to an electric source, which will cause current to go through the SMA wire and which will then heat up the SMA wire.

Icardi has made a reversible actuator that is made of two SMA wires in a elastomer beam [10]. The SMA wires are trained in such a way that when an electric current is applied, the wires deform to a bending shape. When these wires are embedded in an elastomer beam and a current goes through the wires, the entire beam bends due to the bending of the wires, see figure 3.11 on the following page.

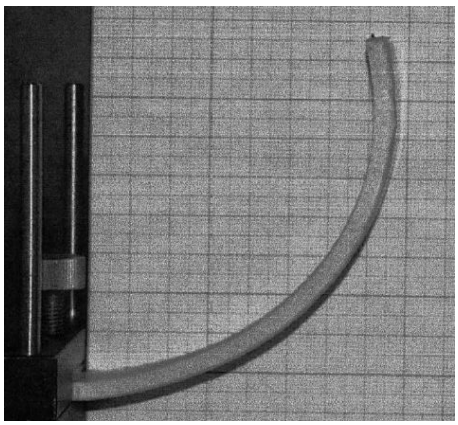

Figure 3.11: SMA wire inside an elastomer beam in activated state [10]

In [31], the authors have also made a reversible actuator using SMA wire. In this case, the actuator is made of a SMA wire and a flexible beam inside a thin-walled elastic tube, see figure 3.12. The actuator reacts in 2 seconds when an electric current is applied. The reversibility of the actuator is achieved by training the SMA wire before application using thermomechanical loading and unloading with resistive heating and a bias spring.

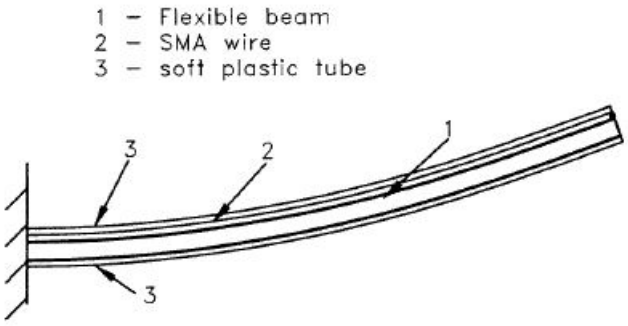

Figure 3.12: SMA wire in a tube [31]

Du et al. report a bending actuator made of a Ni-Ti SMA wire in an elastic substrate [5]. The SMA wire was pre-treated by immersion in hot water and cooling in air to get the memeory effect. The bending of the actuator is caused by the fact, that when an electric stimulus is applied, the temperature increases in the actuator. When a certain temperature is reached, the SMA wires contracts, whereas the elastric subtrate stays the same. This difference in length cause the bending. One disadvantage of this actuator however is that it is not reversible.

Mineta et al. have also made an actuator with Ni-Ti SMA wire. In this case, the actuator is made of Ni-Ti SMA wire in a bias coil spring which is embedded in a polyurethane tube. When current is applied, the actuator shows bending behavior. When the stimulus is removed, the actuator deforms back to its original shape due to the bias coil.

3.4 Water/Humidity

3.4.1 Polymers

Gao et al. have made a multi-responsive bilayer made of GO/PVDF that responds to thermal, IR and moisture stimulus. When the moisture stimulus is applied, the GO layer absorbs water which leads to volume expansion whereas the PVDF layer does not deform. This leads to bending towards the PVDF layer with a strain of 0.25 %. When the stimulus is removed, the bilayer deforms back to its

original flat shape.

Mao et al. have made a device which will bend [18]. This device consists of a hydrogel which is confined between a SMP layer (Grey60) and an elastomer (Tangoblack). These two layers are connected to each other via multiple columns. When the hydrogel comes into contact with water, it wants to expand in all directions, however the columns limit the expansion only in one direction. If the beam is then heated up to 75 °C, the stiffness of the SMP layer decreases compared to the stiffness of the elastomer. This difference in the stiffness will cause the beam to bend. The thinner the elastomer, the higher the bending curvature.

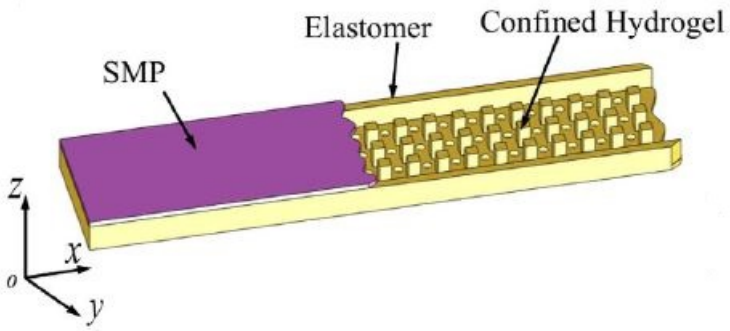

Figure 3.13: Hydrogel between a SMP and an elastomer[18]

Song et al. have developed a bilayer system, which has an active polyurethane (PU) elastomer layer attached to a passive layer [29]. When the bilayer system is made wet, the active PU layer expands, whereas the passive layer does not. This causes a bending deformation of the bilayer. The expansion is controlled by using two moisture-cured polyurethane (PU) elastomers. One of these PU elastomer is water-swellable, whereas the other is not. By playing with the the ratio of these two elastomers in the active layer, one can control the expansion ratio. Furthermore, if one attaches this PU elastomer to a SMP layer, you have 2 active layers, since the SMP layer reacts to a heat stimulus, see figure 3.14.

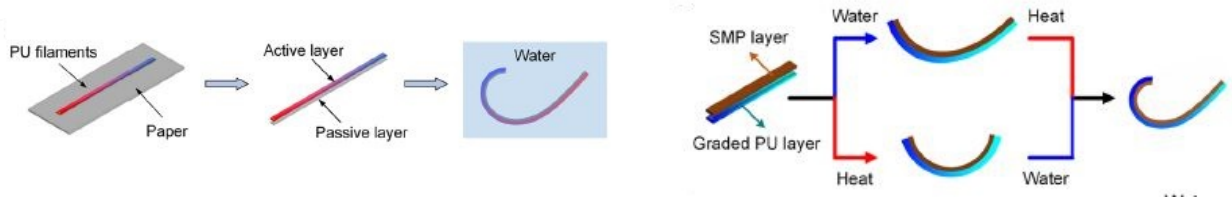

Figure 3.14: Active PU layer with a passive layer (left) and Active PU layer with an active SMP layer (right) [29]

Another stimulus to which the actuator made by Wang et al. responds to, is humidity. When one side of the film is exposed to humid air, a hydrated swollen layer is formed. The non-exposed side of the film is however in a non-swollen sate. This difference in swelling of the sides causes the film to bend in 2 seconds. When the humidity stimulus is removed, the film deforms back to its flat shape within one minute [33].

As explained in section 3.1.1, Gao et al. have made a bilayer which is made of polyvinylidene fluoride (PVDF) and graphene oxide (GO) layers. However, contrary to the elongation of PVDF due to thermal stimulus. The bilayer can bend when moisture is applied. This will cause volume expansion of the GO layer, which then leads to bending, since the PVDF layer does not elongate. So one could use only the GO layer in combination with moisture as stimulus for a zero-torque joint.

Similar to the actuator explained in the previous section, Xiang et al. have also made an actuator using graphene oxide (GO) that reacts to humidity stimulus [37]. However, in this case the GO was combined with PVA-co-PE nanofibers (NFs) and silver nanowires (AgNWs). The working principle of this actuator is similar to the working principle explained in the previous section, which is the absorption/desoprtion of water, which leads to expansion/contraction of the layer, see figure 3.15. This actuator has a response time of 1 second and is reversible.

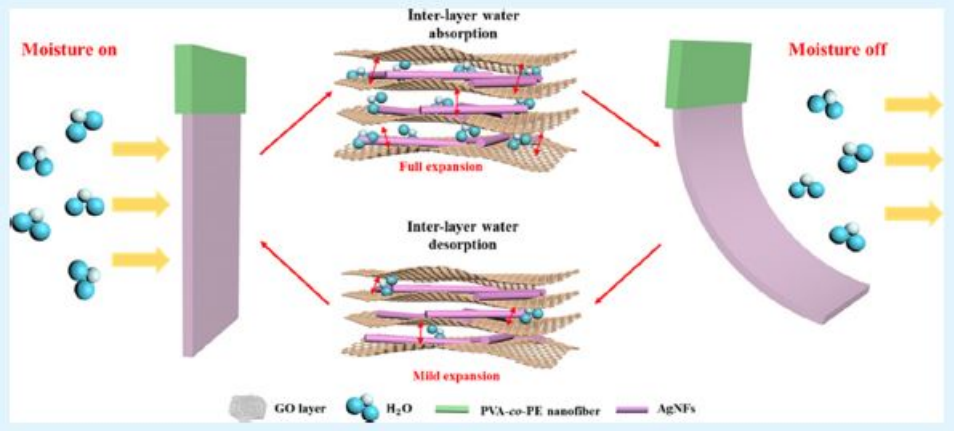

Figure 3.15: Moisture responsive actuator [37]

Wang et al. have also made an actuator that is made of GO that responds to humidity stimulus [34]. This actuator is also responsive to chemical stimulus, see figure 3.16. In this case, the actuator is made of GO and polydimethylsiloxane (PDMS) layers. The GO layer responds to moisture, whereas the PDMS layer responds to alkane. This section explains the humidity stimulus. When the humidity stimulus is applied, the GO layer is the active layer, which means that it expands, whereas the PDMS layer stays the same. This difference in expansion leads to the bending behavior. The response time is 7 seconds.

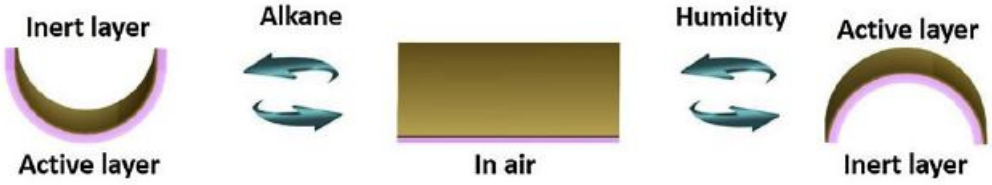

Figure 3.16: Dual stimuli responsive actuator [34]

Qin et al. have made an actuator that responds to water/moisture stimulus [24]. The actuator is made of polyvinyl alcohol (PVA) nanofibers cut into different strips. When the stimulus is applied, the strips can bend, twist, or rotate. When the deformed actuator is immersed in ethanol for 5 seconds, it will restore to its original flat shape.

As explained in section 3.1.1, Wei et al. have made multi-stimulus actuator that is made of Nafion-Polypropylene-Polydimethylsiloxane (PDMS)/Graphite layers [35]. This section presents the humidity stimulus. When this actuator is in a humid environment, the Nafion layer absorbs water molecules. This absorption results in swelling of the Nafion layer, whilst the PDMS/Ghraphite layer stays the same. This leads to bending of the actuator within 5 seconds.

In [23], the authors present a hydrogel strip that can bend when immersed in water within 50 s. The cross-sectional shape of the strip is a half circle. However, if it is kept in water longer, it deforms back to the original shape.

3.5 pH-stimulus

3.5.1 Polymers

Dai et al. have made a pH-responsive actuator [4]. It is made of a Lignin-based hydrogel. Using this hydrogel, the authors made strips. When the strip was immersed in HCl, it obtained a bent shape. When the strip was immersed in KOH, it restored its original shape, see figure 3.17. The calculated strain for this actuator is 7.5 %. The authors report that this actuator shows reversibility, meaning that it can be bent and unbent many times.

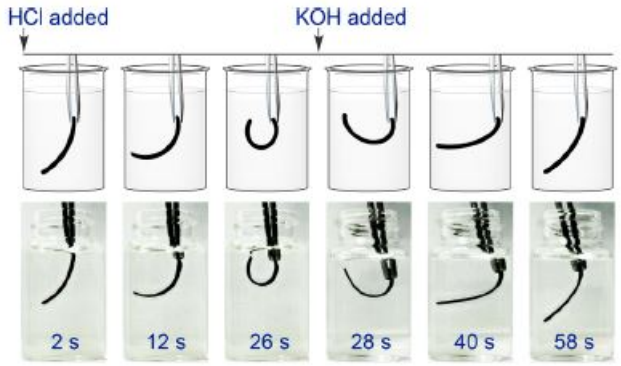

Figure 3.17: pH-responsive actuator [4]

3.6 Chemical

3.6.1 Polymers

The actuator made by Wang et al. can also react to NH_3 and HCl gasses. Exposure to NH_3 gas causes the deprotonation of the PPYNPs. This increases the hydrophobicity of the PPYNPS, which means that the Agar absorobs water from the nanoparticles. This absorption cause the swelling of Agar, which leads to the bending behavior. Contrarily, when the film is exposed to HCl gas, the PPYNPs get protonated. This means that the hydrophilicity of the PPYNPs increases. This means that the nanoparticles absorb the water, which leads to swelling.

As explained is section 3.4.1, Wang et al. have made an actuator that responds to humidity and chemical stimulus [34]. This section explains the chemical stimulus. When the actuator is exposed to alkane, the active PDMS adsorps the alkane molecules. As a result, this layer swells. The GO layer is inert. This leads to bending of the actuator. The response time is 16 seconds.

Zheng et al. have made a reversible actuator that responds to alcohol [38]. It is made of PDMS, where one side of the PDMS sheet is treated with UV/O_3. When the treated side is then exposed to ethanol vapor, the sheet curls toward the untreated side, see figure 3.18 on the following page. The response time is 10 seconds.

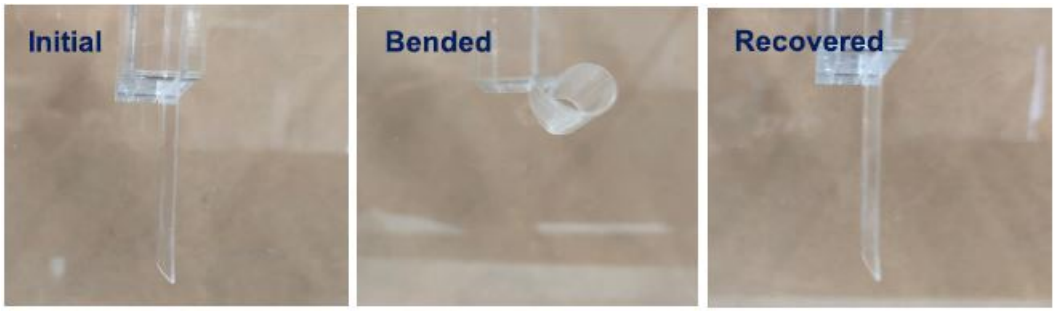

Figure 3.18: Alcohol responsive actuator [38]

3.7 Overview of the findings

An overview of the findings is presented in table 3.1 on the following page. The table lists all the relevant properties of the findings:

Materials: What material is used?

Stimulus: What stimulus does the material react to?

Response time: How much time does the material need to obtain the fully deformed shape when the stimulus is applied?

(Un)-thetered: Is the stimulus applied at the material itself like an electrical stimulus or is it applied from a distance like a thermal stimulus?

Reversible: Is the behavior reversible or not?

Strain: How much strain does the material achieve due to the stimulus?

Nr.	Reference	Material	Stimulus	Response Time (s)	(Un)-Thetered	Reversible?	Strain (%)
1	[11]	Tango+, Verocyan & Veroyellow	Light	30	Unthetered	Not by itself	12.5
2	[6]	GO/PVDF bilayer	Thermal, Moisture, Light	2	Both	Yes	0.2/0.16/0.25
3	[18]	Hydrogel between SMP/Elastomer	Water	10	Thetered	Yes	–
4	[15]	SMA wire in silicon rubber matrix	Thermal, Electrical	10	Both	Yes	18
5	[29]	PU elastomer on SMP (Bilayer)	Moisture, Thermal	600	Both	Not by itself	–
6	[33]	PPYNPs and Agar	Moisture, Chemical, Thermal, Light	2, 1, 1, 1	Both	Yes	0.09
7	[30]	SMP fibers (Veroclear) in elastomer matrix (Tangoplus)	Thermal	120	Unthetered	Yes	13.5
8	[32]	Elastomer (rubber) + SMP (c-copolymer)	Thermal	30	Unthetered	Not by itself	200
9	[21]	LCN/PDMS bilayer	Light	2	Unthetered	Yes	–
10	[25]	c-EVA in PU	Thermal	–	Unthetered	Yes	30
11	[22]	SMPU with dibutyl adipate (DBA)	Thermal, Electrical	5	Both	Not by itself	4
12	[4]	all-lignin-based hydrogel	pH	27	Thetered	Yes	7.5
13	[24]	Polyvinyl alcohol	Moisture	0.15	Thetered	Yes	3.8
14	[35]	Nafion-Polypropylene-PDMS/Graphite Multilayer	Optical, Thermal, Moisture	0.5, 31, 5	Unthetered	Yes	–
15	[16]	Hydrogel	Hot Moisture	9	Thetered	Yes	5
16	[17]	Ionogel Graphene Composite	Electrical	5	Thetered	Yes	–
17	[37]	AgNWs/NFs/GO composite	Moisture	1.2	Thetered	Yes	–
18	[34]	GO/PDMS layers	Moisture, Chemical	7	Thetered	Yes	2.6
19	[38]	UV/O3 treated PDMS & TENG	Chemical	10	Unthetered	Yes	15.7
20	[7]	polyNIPAM/GO	Thermal, Light	22, 17	Unthetered	Yes	5.8
21	[10]	SMA wires in Elastomer	Electrical	–	Thetered	Yes	4
22	[31]	SMA wire in tube	Electrical	2	Thetered	Yes	3
23	[14]	PMAAc/SA IPN hydrogel	Electrical	25	Thetered	Yes	1.31
24	[12]	Al Nc hydrogel	Electrical	50	Thetered	Yes	1.45
25	[3]	GO/PNIPAM bilayer	Light	120	Unthetered	Yes	2.75
26	[5]	NiTi SMA wires in PVC	Electrical	6	Thetered	Yes	4
27	[19]	NiTi SMA wire with a bias	Electrical	–	Thetered	Yes	–
28	[23]	Hydrogel	Moisture	50	Unthetered	Yes	–

Table 3.1: Overview of the findings

Chapter 4 Performance grading

In order to determine which result is the most useful to make a zero-stiffness joint, one needs to grade these results according to a certain criterion. In this section, a performance criteria will be presented. The sources will be graded in the following table using relative grading. This means that the best result gets the highest grade whereas the worst result gets the lowest grade. The most relevant properties for the application in a zero-stiffness joint are the response time, strain and reversibility. These properties will therefore be graded.

Response time: The source with the a response time between 1 - 5 seconds will get a grade of 10, a response time between 6 - 10 seconds gets a 7, a response time between 11 - 60 seconds gets a 5 and anything above 60 seconds gets a 1.

Strain: The source with a strain higher than 10 % gets a grade of 10, a strain between 6 - 10 % gets a 7, a strain between 2 - 5 gets a 5 and a strain between 0 and 2 % will be graded a 1.

Reversibility: The source which gives materials that show reversible behavior to the stimulus gets a 5, whereas if it is not reversible, it gets a 1. When finding sources, reversibility was used as a criterion for the source to match. Most of the sources show reversible behavior. However, there are some sources that do not show this reversible behavior - but are good for the understanding of smart materials - that are included in the findings as well. Therefore, reversibility is also graded to take these sources into account. That is also the reason that the grade for reversibility is either 5 or 1. Therefore, reversibility should not be the most influential factor in the total grading.

Total: The total grade is a weighted sum of 3 different criteria, in which the strain accounts for 50 % of the grade, the response time for 35 % and reversibility for 15 %.

The total grading table can be found on the following page.

Nr.	Reference	Material	Response Time	Strain	Reversibility	Total
1	[11]	Tango+, Verocyan & Veroyellow	5	10	1	6.9
2	[6]	GO/PVDF bilayer	10	1	5	4.8
3	[18]	Hydrogel between SMP/Elastomer	7	–	5	3.2
4	[15]	SMA wire in silicon rubber matrix	7	10	5	8.2
5	[29]	PU elastomer on SMP (Bilayer)	1	–	1	1
6	[33]	PPYNPs and Agar	10	1	5	4.8
7	[30]	SMP fibers (Veroclear) in elastomer matrix (Tangoplus)	1	10	5	6
8	[32]	Elastomer (rubber) + SMP (c-copolymer)	5	10	1	6.9
9	[21]	LCN/PDMS bilayer	10	–	5	4.3
10	[25]	c-EVA in PU	–	10	5	5.8
11	[22]	SMPU with dibutyl adipate (DBA)	10	5	1	6.2
12	[4]	all-lignin-based hydrogel	5	7	5	6
13	[24]	Polyvinyl alcohol	10	5	5	6.8
14	[35]	Nafion-Polypropylene-PDMS/Graphite Multilayer	10	–	5	4.3
15	[16]	Hydrogel	7	5	5	5.7
16	[17]	Ionogel Graphene Composite	10	–	5	4.3
17	[37]	AgNWs/NFs/GO composite	10	–	5	4.3
18	[34]	GO/PDMS layers	7	5	5	5.7
19	[38]	UV/O3 treated PDMS & TENG	7	10	5	8.2
20	[7]	polyNIPAM/GO	5	7	5	6
21	[10]	SMA wires in Elastomer	–	5	5	3.3
22	[31]	SMA wire in tube	10	5	5	6.8
23	[14]	PMAAc/SA IPN hydrogel	5	1	5	3
24	[12]	Al Nc hydrogel	5	1	5	3
25	[3]	GO/PNIPAM bilayer	1	5	5	3.6
26	[5]	NiTi SMA wires in PVC	7	5	5	5.7
27	[19]	NiTi SMA wire with a bias	–	–	5	1
28	[23]	Hydrogel	5	–	5	2.5

Table 4.1: Performance criteria for the findings

Chapter 5 Discussion

This review presents materials that respond to an external stimulus. The main objective of this review is to find alternative materials that could be used to make a joint that works as the Hygromorphic Rotational Actuator (HRA) [13].

It is interesting to note that some of the materials found, shrink when the stimulus is applied. This is in contrast with the behavior of the HRA, where the wooden sheet elongates. The reason for also considering materials that shrink is that instead of constraining the center of sheet and elongating the sheet as in the HRA, one could also constrain the vertical outer edges and shrink the material. This can not be said with certainty, however it is interesting do further research on this.

There are many different smart materials found. It should be noted that these materials are not the only materials that could replace the wooden sheet in the HRA. However, these materials do give a clear idea of what the possibilities are with smart materials. For instance, in cases where a hydrogel is used as an expanding material, any other hydrogel, gas, liquid or material that expands/swells could be used. Or in case where SMA wires are used, one could potentially use SMP fibers or vice versa.

The findings of this review do not give materials that elongate or shrink specifically when the stimulus is applied. However, these materials show a deformation such as bending or helical shape. What is of use, is the underlying working principle of the deformation. The deformation is caused by elongation or shrinkage of some material within the actuator, which can be used. In bilayer systems, one layer usually expands, whereas the other shrinks or stays the same, which causes the bending behavior. For the use in HRA, one could only use the expanding layer which can replace the wooden sheet. Or one could use SMA wires or SMP fibers inside a matrix, that only elongate when a stimulus is applied. Another possible way is using the principle of [30], where the fibers are inserted in a matrix with an angle. When the stimulus is then applied, the device will rotate. This may have the advantage that no constraints are required. This principle works for an actuator application, however it can not be said with certainty that it will work for a joint as well. Therefore, it is an interesting principle that can be tested with initial prototypes in the research phase.

In case of SMA wires, it is interesting to note that all of them work similarly. They all deform when they are heated, which can be done thermally or electrically. These wires can be inserted in different matrix materials which then deform due to the deformation of the SMA wires. In the case of the joint, one can train the SMA wire in such a way that it either elongates or shrinks when it is heated up. If these trained wires are then inserted in matrix, the whole matrix will deform when it is activated which corresponds to the working principle of the HRA.

When looking at stimuli, it can be observed that some stimuli are more difficult to apply than the others. Some hydrogels for instance sometimes not require only water, but the material needs to be treated in certain chemicals before every use. This limits the real-life applications of the material.

For the grading table, it should be noted that there are two materials that are better than the others. However, the rest of the materials are close to each other with the total grade. This is due to the fact that some data could not be obtained from the findings. When it comes to time, it was generally easier to get that from the source. However, for the strain, it has not been directly reported. Most of the times, it was either the bending angle or bending curvature. So some calculations had to be

made to get the strain. All these uncertainties give inaccuracy to the performance criteria. However in order to pick from materials with close total grades, one should look at the strain, since the strain will give the highest zero-stiffness range and that is the main objective of a zero-torque joint.

Chapter 6 Conclusion

The objective of this report is to give an overview of different smart materials along with their corresponding stimuli. This work gives a clear indication of what kind of smart materials there are and what their possibilities are. This review is done to find materials that can replace the wooden sheet in the Hygromorphic Rotaional Actuator (HRA). Therefore, the main properties to look for are the strain, response time and reversibility of materials. A performance criteria is given in which all these properties are graded for all the sources. From this criteria, it is found that the best materials for the use in the HRA are; a SMA wire inside a matrix that responds to thermal or electrical stimulus or UV/O_3 treated PDMS that responds to alcohol. However, it should be noted that this result does not dismiss all the other materials that are found. They can also be used.

Appendix A Extra data for strain calculation

The strain presented in Chapter 3, has not always been directly reported in the used papers. However, most of the papers did give the dimensions of the actuator and bending angles or curvature, which can be seen in table A.1 on the following page. This data is then used to calculate the strain with the following beam equations:

$$L = \rho\theta \tag{A.1}$$

$$\epsilon = \frac{y}{\rho} \tag{A.2}$$

L is the length of the beam, ρ is the radius of curvature and θ is the bending angle. The strain is given by ϵ and y is the distance from the center of the beam to the top, i.e. half the thickness of the beam.

It should be noted that table A.1 on the next page is not entirely filled. The main purpose of this table is to obtain the information to calculate the strain. However, some of the sources did not provide sufficient information, which has lead to the table missing some of the information.

Table A.1: Extra data of the findings

Nr.	Reference	Material	Bending angle/curvature/ROC	Length (mm)	Thickness (mum)	Dimensions (LxBxH) (mm)
1	[11]	Tango+, Verocyan & Veroyellow	–	40	–	40x5.5x2
2	[6]	GO/PVDF bilayer	5, 3.89, 6.3 cm^{-1}	10	8	10x1
3	[18]	Hydrogel between SMP/Elastomer	145 deg	–	–	–
4	[15]	SMA wire in silicon rubber matrix	ROC = 22 mm	45	–	45x15x8
5	[29]	PU elastomer on SMP (Bilayer)	–	–	–	–
6	[33]	PPYNPs and Agar	1.1, 0.96, 1.02, 1.05 cm^{-1}	45	15.7	45x15
7	[30]	SMP fibers (Veroclear) in elastomer matrix (Tangoplus)	90 m^{-1}	50	–	50x8x3
8	[32]	Elastomer (rubber) + SMP (c-copolymer)	–	–	–	–
9	[21]	LCN/PDMS bilayer	–	–	–	microns
10	[25]	c-EVA in PU	–	–	–	50x40x1
11	[22]	SMPU with dibutyl adipate (DBA)	–	–	–	40x10
12	[4]	all-lignin-based hydrogel	216 deg	–	–	50x15x2
13	[24]	Polyvinyl alcohol	25.3 cm^{-1}	–	30	15x5
14	[35]	Nafion-Polypropylene-PDMS/Graphite Multilayer	325/225 deg	–	–	5x10
15	[16]	Hydrogel	289 deg	–	–	50x10x1
16	[17]	Ionogel Graphene Composite	–	25	–	–
17	[37]	AgNWs/NFs/GO composite	140 deg	–	–	–
18	[34]	GO/PDMS layers	10 cm^{-1}	–	52	15x1
19	[38]	UV/O3 treated PDMS & TENG	360 deg	–	1500	30x20
20	[7]	polyNIPAM/GO	200 deg	–	–	30x10x1
21	[10]	SMA wires in Elastomer	–	150	–	150x20x5
22	[31]	SMA wire in tube	–	380	–	–
23	[14]	PMAAc/SA IPN hydrogel	75 deg	–	–	20x5x0.4
24	[12]	Al Nc hydrogel	50 deg	–	–	30x3x1
25	[3]	GO/PNIPAM bilayer	2 cm^{-1}	50	–	–
26	[5]	NiTi SMA wires in PVC	–	–	–	80x20x0.32
27	[19]	NiTi SMA wire with a bias	60 deg	5	–	–
28	[23]	Hydrogel	0.12 mm^{-1}	15	–	–

References

[1] *About Compliant Mechanisms*. URL: https://www.compliantmechanisms.byu.edu/about-compliant-mechanisms.

[2] Sovan Lal Banerjee et al. "Ag NPs incorporated self-healable thermoresponsive hydrogel using precise structural "Interlocking" complex of polyelectrolyte BCPs: A potential new wound healing material". In: *Chemical Engineering Journal* 405 (2021), p. 126436. ISSN: 1385-8947. DOI: https://doi.org/10.1016/j.cej.2020.126436. URL: https://www.sciencedirect.com/science/article/pii/S138589472032564X.

[3] Ze Chen et al. "Graphene oxide/poly (N-isopropylacrylamide) hybrid film-based near-infrared light-driven bilayer actuators with shape memory effect". In: *Sensors and Actuators B: Chemical* 255 (2018), pp. 2971–2978. ISSN: 0925-4005. DOI: https://doi.org/10.1016/j.snb.2017.09.119. URL: http://www.sciencedirect.com/science/article/pii/S0925400517317859.

[4] Lin Dai et al. "All-Lignin-Based Hydrogel with Fast pH-Stimuli Responsiveness for Mechanical Switching and Actuation". In: *Chemistry of Materials* 32.10 (2020), pp. 4324–4330. DOI: 10.1021/acs.chemmater.0c01198. eprint: https://doi.org/10.1021/acs.chemmater.0c01198. URL: https://doi.org/10.1021/acs.chemmater.0c01198.

[5] Yong Du et al. "Dynamic characteristics of planar bending actuator embedded with shape memory alloy". In: *Mechatronics* 25 (2015), pp. 18–26. ISSN: 0957-4158. DOI: https://doi.org/10.1016/j.mechatronics.2014.11.001. URL: http://www.sciencedirect.com/science/article/pii/S095741581400169X.

[6] Tiantian Gao et al. "An intelligent film actuator with multi-level deformation behaviour". In: *Nanoscale Horiz.* 5 (8 2020), pp. 1226–1232. DOI: 10.1039/D0NH00268B. URL: http://dx.doi.org/10.1039/D0NH00268B.

[7] Xiaomin He et al. "Dual-stimulus bilayer hydrogel actuators with rapid, reversible, bidirectional bending behaviors". In: *J. Mater. Chem. C* 7 (17 2019), pp. 4970–4980. DOI: 10.1039/C9TC00180H. URL: http://dx.doi.org/10.1039/C9TC00180H.

[8] Larry L. Howell. "Introduction to Compliant Mechanisms". In: *Handbook of Compliant Mechanisms*. John Wiley & Sons, Ltd, 2013. Chap. 1, pp. 1–13. ISBN: 9781118516485. DOI: https://doi.org/10.1002/9781118516485.ch1. eprint: https://onlinelibrary.wiley.com/doi/pdf/10.1002/9781118516485.ch1. URL: https://onlinelibrary.wiley.com/doi/abs/10.1002/9781118516485.ch1.

[9] W.M. Huang et al. "Shape memory materials". In: *Materials Today* 13.7 (2010), pp. 54–61. ISSN: 1369-7021. DOI: https://doi.org/10.1016/S1369-7021(10)70128-0. URL: http://www.sciencedirect.com/science/article/pii/S1369702110701280.

[10] U. Icardi. "Large bending actuator made with SMA contractile wires: Theory, numerical simulation and experiments". In: *Composites Part B: Engineering* 32 (Apr. 2001), pp. 259–267. DOI: 10.1016/S1359-8368(00)00062-7.

[11] Hoon Jeong et al. "Multicolor 4D printing of shape-memory polymers for light-induced selective heating and remote actuation". In: *Scientific Reports* 10 (Apr. 2020), p. 6258. DOI: 10.1038/s41598-020-63020-9.

[12] Haoyang Jiang et al. "Tough and electro-responsive hydrogel actuators with bidirectional bending behavior". In: *Nanoscale* 11 (5 2019), pp. 2231–2237. DOI: 10.1039/C8NR07863G. URL: http://dx.doi.org/10.1039/C8NR07863G.

[13] Sebastiaan Joosten, Giuseppe Radaelli, and Heike Vallery. “Passive autonomy: hygromorphic rotational actuators”. In: *Smart Materials and Structures* (Nov. 2020). DOI: 10.1088/1361-665x/abcf1e. URL: https://doi.org/10.1088/1361-665x/abcf1e.

[14] Seon Jeong Kim et al. “Bending behavior of hydrogels composed of poly(methacrylic acid) and alginate by electrical stimulus”. In: *Polymer International* 53.10 (2004), pp. 1456–1460. DOI: https://doi.org/10.1002/pi.1560. eprint: https://onlinelibrary.wiley.com/doi/pdf/10.1002/pi.1560. URL: https://onlinelibrary.wiley.com/doi/abs/10.1002/pi.1560.

[15] Zhengjie Li, Rong Huang, and Zishun Liu. “A Periodic Deformation Mechanism of a Soft Actuator for Crawling and Grasping”. In: *Advanced Materials Technologies* 4.12 (2019), p. 1900653. DOI: https://doi.org/10.1002/admt.201900653. eprint: https://onlinelibrary.wiley.com/doi/pdf/10.1002/admt.201900653. URL: https://onlinelibrary.wiley.com/doi/abs/10.1002/admt.201900653.

[16] Jian Liu et al. “Gradient porous PNIPAM-based hydrogel actuators with rapid response and flexibly controllable deformation”. In: *Journal of Materials Chemistry C* 8 (June 2020). DOI: 10.1039/D0TC00139B.

[17] Lu and Chen. “Flexible and Electroactive Ionogel Graphene Composite Actuator”. In: *Materials* 13 (Feb. 2020), p. 656. DOI: 10.3390/ma13030656.

[18] Y. Mao et al. “3D Printed Reversible Shape Changing Components with Stimuli Responsive Materials”. In: *Scientific Reports* 6 (Apr. 2016), p. 24761. DOI: 10.1038/srep24761.

[19] Takashi Mineta et al. “An active guide wire with shape memory alloy bending actuator fabricated by room temperature process”. In: *Sensors and Actuators A: Physical* 97-98 (2002). Selected papers from Eurosenors XV, pp. 632–637. ISSN: 0924-4247. DOI: https://doi.org/10.1016/S0924-4247(02)00021-3. URL: http://www.sciencedirect.com/science/article/pii/S0924424702000213.

[20] Farhang Momeni et al. “A review of 4D printing”. In: *Materials & Design* 122 (2017), pp. 42–79. ISSN: 0264-1275. DOI: https://doi.org/10.1016/j.matdes.2017.02.068. URL: http://www.sciencedirect.com/science/article/pii/S0264127517302034.

[21] Marina Pilz da Cunha et al. “On Untethered, Dual Magneto- and Photoresponsive Liquid Crystal Bilayer Actuators Showing Bending and Rotating Motion”. In: *Advanced Optical Materials* 7.7 (2019), p. 1801604. DOI: https://doi.org/10.1002/adom.201801604. eprint: https://onlinelibrary.wiley.com/doi/pdf/10.1002/adom.201801604. URL: https://onlinelibrary.wiley.com/doi/abs/10.1002/adom.201801604.

[22] Suphassa Pringpromsuk, Hong Xia, and Qing-Qing Ni. “Multifunctional stimuli-responsive shape memory polyurethane gels for soft actuators”. In: *Sensors and Actuators A: Physical* 313 (2020), p. 112207. ISSN: 0924-4247. DOI: https://doi.org/10.1016/j.sna.2020.112207. URL: http://www.sciencedirect.com/science/article/pii/S0924424720307457.

[23] Li Qi et al. “Kinetics-induced morphing of 3D-printed gel structures based on geometric asymmetry”. In: *Journal of Applied Mechanics* 87 (Apr. 2020), pp. 1–25. DOI: 10.1115/1.4046920.

[24] Juanrong Qin et al. “Nanofibrous Actuator with an Alignment Gradient for Millisecond-Responsive, Multidirectional, Multimodal, and Multidimensional Large Deformation”. In: *ACS Applied Materials & Interfaces* 12.41 (2020). PMID: 32945656, pp. 46719–46732. DOI: 10.1021/acsami.0c13594. eprint: https://doi.org/10.1021/acsami.0c13594. URL: https://doi.org/10.1021/acsami.0c13594.

[25] JE Rodriguez et al. “Cross-linked ethylene-vinyl acetate – poly(urethane) temperature-memory composite actuator”. In: *Journal of Composite Materials* 54.28 (2020), pp. 4441–4455. DOI: 10.1177/0021998320933664. eprint: https://doi.org/10.1177/0021998320933664. URL: https://doi.org/10.1177/0021998320933664.

[26] Mark Schenk and Simon D Guest. "On zero stiffness". In: *Proceedings of the Institution of Mechanical Engineers, Part C: Journal of Mechanical Engineering Science* 228.10 (2014), pp. 1701–1714. DOI: 10.1177/0954406213511903. eprint: https://doi.org/10.1177/0954406213511903. URL: https://doi.org/10.1177/0954406213511903.

[27] Mel Schwartz. *Smart materials*. CRC press, 2008.

[28] N. Simiriotis et al. "Shape control and design of aeronautical configurations using shape memory alloy actuators". In: *Computers & Structures* 244 (2021), p. 106434. ISSN: 0045-7949. DOI: https://doi.org/10.1016/j.compstruc.2020.106434. URL: https://www.sciencedirect.com/science/article/pii/S0045794920302376.

[29] Zhengyi Song et al. "Biomimetic Nonuniform, Dual-Stimuli Self-Morphing Enabled by Gradient Four-Dimensional Printing". In: *ACS Applied Materials & Interfaces* 12.5 (2020). PMID: 31920076, pp. 6351–6361. DOI: 10.1021/acsami.9b17577. eprint: https://doi.org/10.1021/acsami.9b17577. URL: https://doi.org/10.1021/acsami.9b17577.

[30] Dong Wang et al. "Effect of temperature on the programmable helical deformation of a reconfigurable anisotropic soft actuator". In: *International Journal of Solids and Structures* 199 (2020), pp. 169–180. ISSN: 0020-7683. DOI: https://doi.org/10.1016/j.ijsolstr.2020.04.028. URL: http://www.sciencedirect.com/science/article/pii/S002076832030144X.

[31] Guoping Wang and Mohsen Shahinpoor. "Design, prototyping and computer simulations of a novel large bending actuator made with a shape memory alloy contractile wire". In: *Smart Materials and Structures* 6.2 (Apr. 1997), pp. 214–221. DOI: 10.1088/0964-1726/6/2/011. URL: https://doi.org/10.1088/0964-1726/6/2/011.

[32] Lin Wang et al. "Controllable Shape Changing and Tristability of Bilayer Composite". In: *ACS Applied Materials & Interfaces* 11.18 (2019), pp. 16881–16887. DOI: 10.1021/acsami.8b21214. eprint: https://doi.org/10.1021/acsami.8b21214. URL: https://doi.org/10.1021/acsami.8b21214.

[33] Taoping Wang et al. "A multi-responsive bidirectional bending actuator based on polypyrrole and agar nanocomposites". In: *J. Mater. Chem. C* 6 (24 2018), pp. 6416–6422. DOI: 10.1039/C8TC00747K. URL: http://dx.doi.org/10.1039/C8TC00747K.

[34] Wei Wang et al. "A complementary strategy for producing moisture and alkane dual-responsive actuators based on graphene oxide and PDMS bimorph". In: *Sensors and Actuators B: Chemical* 290 (2019), pp. 133–139. ISSN: 0925-4005. DOI: https://doi.org/10.1016/j.snb.2019.03.117. URL: http://www.sciencedirect.com/science/article/pii/S0925400519304836.

[35] Yao Wei et al. "Smart Devices Based on the Soft Actuator with Nafion-Polypropylene-PDMS/Graphite Multilayer Structure". In: *Applied Sciences* 10 (Mar. 2020), p. 1829. DOI: 10.3390/app10051829.

[36] Jiangtao Wu et al. "Multi-shape active composites by 3D printing of digital shape memory polymers". In: *Scientific Reports* 6 (Apr. 2016), p. 24224. DOI: 10.1038/srep24224.

[37] Chenxue Xiang et al. "Flexible and Super-Sensitive Moisture-Responsive Actuators by Dispersing Graphene Oxide into Three-Dimensional Structures of Nanofibers and Silver Nanowires". In: *ACS Applied Materials & Interfaces* 12.2 (2020). PMID: 31867950, pp. 3245–3253. DOI: 10.1021/acsami.9b20365. eprint: https://doi.org/10.1021/acsami.9b20365. URL: https://doi.org/10.1021/acsami.9b20365.

[38] Li Zheng et al. "Dual-Stimulus Smart Actuator and Robot Hand Based on a Vapor-Responsive PDMS Film and Triboelectric Nanogenerator". In: *ACS Applied Materials & Interfaces* 11.45 (2019). PMID: 31642666, pp. 42504–42511. DOI: 10.1021/acsami.9b15574. eprint: https://doi.org/10.1021/acsami.9b15574. URL: https://doi.org/10.1021/acsami.9b15574.

[39] Bo Zhu et al. "A Novel Method of Self-Healing in Cementitious Materials by Using Polyacrylic Hydrogel". In: *KSCE Journal of Civil Engineering* 24 (Aug. 2020). DOI: 10.1007/s12205-020-0090-6.